ASSESSMENT OF RADIOLOGICAL HAZARDS DUE TO RADIONUCLIDES IN SOIL AND KHAT (*CATHA EDULIS*) FROM DADAMU SUB-COUNTY IN ARUA DISTRICT, UGANDA

BY

OKELLO ANTHONY

21/U/14541/GMSP/PE

A DISSERTATION SUBMITTED TO THE DIRECTORATE OF RESEARCH AND GRADUATE TRAINING IN PARTIAL FULFILMENT OF THE REQUIREMENTS FOR THE AWARD OF THE DEGREE OF MASTER OF SCIENCE IN PHYSICS OF KYAMBOGO UNIVERSITY

NOVEMBER, 2025

DECLARATION

I, Okello Anthony, do hereby declare that this dissertation contains my original work and has not been presented to any University or academic institution for any academic award.

Signed……..…Date**:**……

APPROVAL

This is to certify that the dissertation entitled ‘Assessment of radiological hazards due to radionuclides in soil and khat (*Catha edulis)* from Dadamu sub-county in Arua district, Uganda’ by Okello Anthony, was developed under our direct supervision. The dissertation is now ready for submission to the graduate school of Kyambogo University for examination with our due approval.

Signature:  Date: 07 November 2025

Dr. Kyeyune Farooq

Signature:…….Date:……

Dr. Ochen William

DEDICATION

I dedicate this work to my beloved mother, the late Lilly Amono, my wife, Amua Rebecca, and my children: Agenorwot Naume, Lakica Jemima, and Nimaro Sarah Prudence.

ACKNOWLEDGEMENT

I extend my sincere gratitude to God for the gifts of wisdom and good health, and without divine intervention, this dissertation wouldn't have been completed. May his name be praised!

I wholeheartedly acknowledge, with special thanks, the supervisory support and advice of my committed supervisors, Dr Kyeyune Farooq and Dr Ochen William, to whom I am deeply indebted. I can't express my gratitude to you in words. May you live longer!

I'm deeply grateful to all the staff members of the Physics Department at Kyambogo University, especially Dr Abedigamba Patrick Oyirwoth and Dr Nsamba Benard, for their valuable advice and support.

I am also thankful to the management of the radiation laboratory of Kyambogo University for giving me access to the equipment. My special recognition goes to Mr Turyahabwa Silver for dedicating his time to training me to operate the high-purity germanium detector. Further appreciation goes to Mr Kawuki Joseph, a senior laboratory technician, for always being available whenever needed.

Lastly, my sincere appreciation goes to my family, friends, Dr Tabu Benard, Mr Opiyo Washington, Mr Omony Robinson, Mr Ochola Francis, and Mr Opiya Paul, all of Gulu University, for their support during the sample collection. Additional appreciation goes to Mr Atiku Rhone of Muni University, who worked as a guide, language translator, and driver during the sample collection.

TABLE OF CONTENTS

DECLARATION.....i

APPROVAL.....ii

DEDICATION..... iii

ACKNOWLEDGEMENT iv

TABLE OF CONTENTS.....v

LIST TABLES.....x

ABSTRACT..... xiii

CHAPTER ONE: INTRODUCTION.....1

1.1 Background of the Study 1

1.2 Statement of the Problem.....3

1.3 Objectives of the study 4

1.3.1 General objective of the study 4

1.3.2 Specific Objectives 4

1.4 Significance of the study 4

1.5 Scope of the Study.....5

CHAPTER TWO: LITERATURE REVIEW.....6

2.1 Introduction.....6

2.2 Sources of radioactivity 6

2.3 Radioactive decay.....8

2.4 Khat.....10

2.5 Migration of radionuclides from soil to plants 13

2.6 Soil-to-plant transfer factor.....13

2.7 Exposure to radionuclides....14
2.8 Health effects due to natural radionuclide exposure....15
2.9 Gamma-ray spectroscopy....16
2.9.1 Scintillation detectors....16
2.9.2 Semiconductor detectors....17
2.10 Performance of the gamma-ray spectrometry system....18
2.11 Related studies about the radioactivity concentration in soil and khat....19
CHAPTER THREE: MATERIALS AND METHODS....21
3.1 Introduction....21
3.2 Study Area....21
3.3 Sample collection....23
3.4 Sample preparation....25
3.5 Gamma-ray spectrometry system setup....27
3.5.1 Energy calibration....28
3.5.2 Efficiency calibration....29
3.5.3 Background radiation count....30
3.5.4 Determination of the activity concentrations of the radionuclides....30
3.6 Soil-to-plant transfer factor....32
3.7 Radiological hazard parameters....32
3.7.1 Radium equivalent activity....33
3.7.2 Absorbed gamma dose rate....33
3.7.3 Annual effective equivalent dose....34
3.7.4 Annual committed effective ingestion dose from khat....34
3.7.5 Excess lifetime cancer risk....35
CHAPTER FOUR: RESULTS AND DISCUSSIONS....37

4.1 Introduction.....37

4.2 Activity concentrations.....37

4.2.1 Soil samples.....37

2.2 Khat samples.....39

4.2.3 Comparison of activity concentrations of ^{232}Th, ^{40}K, and ^{226}Ra in soil and khat.....41

4.3 Soil-to-plant transfer factors.....44

4.4 Radiological hazard parameters in soil.....46

4.5 Radiological hazard parameters in khat.....49

4.6 Annual organ equivalent dose to different body parts.....51

4.7 Statistical Analysis.....54

4.7.1 Pearson correlation analysis.....54

4.7.2 Principal component analysis.....56

4.7.3 Hierarchical cluster analysis.....58

CHAPTER FIVE: CONCLUSION AND RECOMMENDATIONS.....60

5.1 Conclusion.....60

5.2 Recommendations.....61

REFERENCES.....62

Appendix A.....71

LIST OF FIGURES

Figure 2.1: The decay chain of Radionuclides of ^{238}U and ^{232}Th 9

Figure 3.1:(a) Map of Uganda, (b) Arua District, and (c) Sample collection points in Dadamu sub-county. 22

Figure 3.2: Soil sample collection using a sampler. 24

Figure 3.3:(a) Powder khat samples in aluminium disks placed in an electric oven and (b) a stainless steel electric grinder for grinding the soil and khat samples.....26

Figure 3.4: The prepared samples of soil and khat are placed in separate rows, ready for analysis. 27

Figure 3.5: The setup of HPGe detector components used to analyse the samples. 27

Figure 3.6: The energy calibration graph produced by the Genie-2000 software. 29

Figure 3.7: The efficiency calibration curve for the HPGe detector used to calculate the activity concentrations of ^{232}Th, ^{40}K, and ^{226}Ra in the samples. 30

Figure 4.1: Average activity concentrations of ^{232}Th, ^{40}K, and ^{226}Ra in soil and khat. 42

Figure 4.2: Average activity concentrations of 40K, ^{232}Th, and ^{226}Ra in (a) soil and (b) khat from different countries. 43

Figure 4.3: Average soil-to-plant transfer factor of ^{232}Th, ^{40}K, and ^{226}Ra from soil to khat from the Dadamu Sub-county. 46

Figure 4.4: Radiological hazards in (a) Soil and Khat in this study and (b) Soils from other countries. The WPLs represent the world's permissible limits of radiological hazards. 47
Figure 4.5: Radiological hazard parameters in khat from different countries. ...51
Figure 4.6: Heat map illustrating Pearson's correlation analysis of activity concentration of radionuclides and the radiological hazard indices in (a) soil and (b) khat. 55
Figure 4.7: Graphical representations of the PCA between the activity concentrations of ^{40}K, ^{226}Ra, and ^{232}Th and the radiological hazard parameters in (a) soil and (b) khat from Dadamu Sub-county.57
Figure 4.8: Dendrograms for the HCA of (a) Soil and (b) Khat from the Dadamu sub-county. 59

LIST TABLES

Table 3.1: Sample collection matrix per location. 24

Table 3.2: The GPS coordinates of the sampling points. 25

Table 3.3: Gamma-ray lines and their corresponding branching ratios used in calculating the activity levels of ^{232}Th, ^{40}K, and ^{226}Ra. 31

Table 4.1: Activity concentrations of ^{232}Th, ^{40}K, and ^{226}Ra in soil from the Dadamu sub-county. 39

Table 4.2: Activity concentrations of ^{232}Th, ^{40}K, and ^{226}Ra in khat from the Dadamu sub-county. 41

Table 4.3: Yearly organ equivalent doses from ingestion of ^{232}Th, ^{40}K, and ^{226}Ra in Khat from Dadamu sub-county. 53

Table A.1: Average activity concentrations of ^{232}Th, ^{40}K, and ^{226}Ra in soil and khat from different countries. 71

Table A.2: The soil-to-plant transfer factors of ^{232}Th, ^{40}K, and ^{226}Ra for soil and khat samples from the Dadamu cub county. 72

Table A.3: The radiological hazard parameters in soil samples from the Dadamu Sub County. 73

Table A.4: Comparison of the radiological hazard parameters in soil in this study with other studies around the world. 74

Table A.5: Radiological hazard parameters due to ingestion of Khat from the Dadamu Sub-county. 75

Table A.6: Average radiological hazard indices calculated from ^{232}Th, ^{40}K, and ^{226}Ra mean concentrations in khat from different countries. 76

Table A.7: The Radiological Toolbox-generated annual organ doses received from ingestion of ^{232}Th, ^{40}K, and ^{226}Ra in khat from the Dadamu-Sub-county. 77

Table A.8: The factor loadings for the Principal components in (a) Soil and (b) Khat. 79

LIST OF ABBREVIATIONS

ADC	Analog-to-Digital Converter
$ACED_{Ing}$	Annual Committed effective Ingestion dose
DL	Duration of Lifetime
DNA	Deoxyribonucleic Acid
ELCR	Excess Lifetime Cancer Risk
FWHM	Full Width at Half-Maximum
GPS	Global Positioning System
HCA	Hierarchical Cluster Analysis
HPGe	High-Purity Germanium
IR_{ing}	Ingestion Rate
MCA	Multi-Channel Analyser
NORM	Naturally Occurring Radioactive Materials
PC	Principal Component
PCA	Principal Component Analysis
RF	Risk Factor
SDG	Sustainable Development Goal
TF	Transfer Factor
UBOS	Uganda Bureau of Statistics
UNSCEAR	United Nations Scientific Committee on Effects of Atomic Radiation
USA	United States of America
USEPA	United States Environmental Protection Agency
WHO	World Health Organisation
WPL	World Permissible Limit

ABSTRACT

Khat chewing has been associated with a range of health risks, such as mental illness, male impotence, emotional instability, lesions, and liver cancer. These risks may be exacerbated when khat (*Catha edulis*) is grown in soils containing elevated levels of primordial radionuclides. This study aimed to determine the concentrations of radionuclides ^{232}Th, ^{226}Ra, and ^{40}K in soil and khat collected from the Dadamu sub-county found in Arua District. It also evaluated the potential radiological risks posed by these elements to human health. A high-purity germanium (HPGe) detector was used to determine the radionuclide concentrations in 11 soil and 11 khat samples. The mean concentrations in soil were 59.16 ± 13.55, 512.05 ± 149.25, and 23.32 ± 5.59 Bq kg^{-1} for ^{232}Th, ^{40}K, and ^{226}Ra, respectively. ^{232}Th and ^{40}K mean activities in the soil exceeded the global permissible limits by 97% and 28%, respectively, while the ^{226}Ra activity level was below the threshold by 33%. In khat samples, the mean activity concentrations were 5.60 ± 1.39, 322.92 ± 72.22, and 7.24 ± 1.56 Bq kg^{-1} for ^{232}Th, ^{40}K, and ^{226}Ra, respectively, which are lower than the global permissible limits by 81%, 19%, and 79%, respectively. Key radiological hazard parameters were computed, including radium equivalent activity (Ra_{eq}), absorbed gamma dose rate (D_R), annual committed effective dose (ACED), and excess lifetime cancer risk (ELCR). While most hazard parameters did not exceed the recommended limits, absorbed gamma dose rates in soil and khat, ACED, and ELCR exceeded safe thresholds, indicating that unregulated consumption of khat from the study area over a long period could elevate the risk of various cancers. Statistical analyses, which included Pearson correlation, hierarchical clustering, and principal component analysis, revealed that ^{232}Th is the primary contributor to the computed radiological hazards. The findings emphasizes the necessity of routine monitoring and regulation of khat growing and consumption in the Dadamu sub-county to protect public health from potential radiation-related risks.

CHAPTER ONE: INTRODUCTION

1.1 Background of the Study

Radionuclides are unstable isotopes that emit ionising radiation and release energy to attain stability (Olagbaju et al., 2021). Soil radioactivity originates from the weathering of bedrock, which serves as a major source of natural radionuclides. During weathering, primordial radionuclides are released into the soil and spread to other environmental components through erosion and dust particles. These radionuclides can be found in varying amounts in environmental components, including soil, water, rocks, and plants (Ajayi et al., 2018). The spread of radioactive substances in soil is non-uniform and depends on several factors, including geographical location, geology, and soil condition (Olagbaju et al., 2021).

Anthropogenic practices such as mining can significantly elevate the concentrations of radioelements in soil and plants (Aparecida et al., 2017). During mining, especially of uranium, phosphate, and gold, these radionuclides are brought to the surface, thereby increasing their availability in the environment. Additionally, the mining process generates waste rocks and tailings that often contain elevated levels of radionuclides. Subsequent leaching of these materials into the soil and groundwater leads to the aggregation of radionuclides in our surroundings (Aparecida et al., 2017). This implies that areas with poorly disposed of mining waste are at high risk of contamination by radionuclides. Traces of uranium and gold have been reported in the Arua district, especially in Vurra, near the Democratic Republic of Congo border and Dadamu Sub-county (Nyakecho & Hagemann, 2024). Additionally, Dadamu sub-county in the past has experienced

small-scale illegal gold mining, though there is no documented record (Nyakecho & Hagemann, 2024).

Radioactive substances in soil are typically drawn in through the plant roots during mineral uptake and subsequently circulated to different parts of the plant through soil-to-plant transfer. Soil radioactivity can expose humans to radiation and directly contaminate agricultural land and its products. The quantity of radioelements transferred from soil to various plant components is expressed as the soil-to-plant transfer factor. Ingestion of radiation-contaminated green plants is a direct pathway by which radioelements can infiltrate the human food chain (Truc et al., 2023).

Khat (*Catha edulis*) is a medicinal plant with an increasing number of users. This evergreen shrub, known for its mild psychoactive properties, grows as a wild plant or is cultivated mainly in Yemen, Somalia, Ethiopia, Uganda, Kenya, and Tanzania. The plant is recognised by different names depending on the country, such as *qaad* (or *jaad*) in Somalia, *miraa* in Kenya, *mubulo* in Tanzania, *khat* in Ethiopia, and *mairungi* in Uganda. People often chew the fresh leaves and stems, ingesting their bioactive components to induce stimulation and a feeling of euphoria. A small proportion of users consume khat by smoking its dried leaves or preparing a drink. Khat consumption has recently increased, especially among high school and university students, at entertainment venues, and among long-distance drivers (Techan, 2021). It is estimated that over 10 million individuals in the Arabian Peninsula and East Africa consume khat everyday (Asfaw et al., 2023), largely due to its effects of enhancing alertness and energy, reducing the need for sex, sleep, and food, increasing tolerance to fatigue, and easing social interaction (Tesfaye et al., 2020).

However, chewing khat grown in areas with high levels of naturally occurring radioactive materials can introduce radionuclides into the human body. Prolonged consumption can lead to the bioaccumulation of carcinogenic radioactive materials in the essential internal organs, like the stomach, pancrease, kidneys, and liver, potentially causing significant organ damage (McColl et al., 2015). Other adverse health effects of long-term khat chewing include oral and lung cancer, central nervous system damage, high blood pressure, mental retardation, stroke, and reduced sex drive (Asfaw et al., 2023). The degree of these effects depends on the absorbed radiation dose and the duration of exposure. The World Health Organisation has set the global safe limit for natural radionuclides in the diet at 0.3 $\mathrm{mSv\,y^{-1}}$ (UNSCEAR, 2000). Therefore, regular monitoring of radionuclide concentrations in soil and plants is essential for detecting radiation contamination early, enabling authorities to implement preventive measures. The world's permissible limit is a benchmark for identifying potential deviations and ensuring adherence to public health guidelines.

1.2 Statement of the Problem

Khat (*Catha edulis*) is widely consumed in parts of Uganda for its stimulant properties. However, its use has been associated with serious health issues such as mental illness, reproductive dysfunction, and cancers of the liver and oesophagus. In Arua District, particularly in Dadamu sub-county, a major khat growing area, there are known uranium ore deposits and a history of artisanal gold mining (Nyakecho et al., 2024). These activities may contribute to the contamination of soil and khat with primordial radionuclides such as ^{232}Th, ^{40}K, and ^{226}Ra. This raises the concern that regular khat consumption could expose users to harmful levels of radionuclides. Reports of rising cases of liver, lung, and oesophagus

cancers in the region have further heightened these concerns, suggesting a potential link to environmental contamination (Sharon et al., 2024). However, there is limited data on radionuclide concentrations in local soil and khat, and the extent to which they contribute to long-term radiological health risks remains unclear. This study, therefore, aimed to establish the concentrations of radionelements in soil and khat from Dadamu sub-county and to determine the likely radiological threats to consumers.

1.3 Objectives of the study

1.3.1 General objective of the study

To assess the radiological hazards due to radionuclides in soil and khat from Dadamu Sub-county in the Arua district of Uganda.

1.3.2 Specific Objectives

The specific objectives of the study were to;

(i) determine the activity concentrations of ^{232}Th, ^{40}K, and ^{226}Ra in soil and khat samples collected from Dadamu sub-county, Arua district.

(ii) estimate the radiological hazard levels associated with ^{232}Th, ^{40}K, and ^{226}Ra in soil and khat samples.

(iii) establish the interconnection between the activity concentrations of ^{232}Th, ^{40}K, and ^{226}Ra and the radiological hazard parameters.

1.4 Significance of the study

This study contributes to Sustainable Development Goal (SDG) 3, which focuses on a healthy environment and uplifting well-being. The study findings can be used to encourage practices such as crop selection, crop rotation, soil testing, and crop testing to reduce harmful radiation in the ecosystem. These practices align with

SDG 15, which emphasises the preservation of biodiversity and healthy ecosystems for agricultural and human well-being. In addition, the results can raise public awareness of the risk of radionuclide exposure from khat consumption. Understanding the concentration levels of these radionuclides in khat can inform policymakers in developing regulatory measures to protect the health of khat consumers, both nationally and internationally.

1.5 Scope of the Study

The study determined the concentrations of ^{226}Ra, ^{232}Th, and ^{40}K in 11 soil and 11 khat samples using a HPGe detector. The concentrations were then used to evaluate the potential risks posed by soil and khat, based on parameters such as Ra_{eq}, annual effective dose equivalent, D_R in air, $ACED_{ing}$, and ELCR. Additionally, the Radiological toolbox software was used to calculate annual radiation exposure to 15 organs of the body. The samples were taken from five randomly chosen khat-growing cells in Dadamu Sub-county, namely Ndriba, Ariwara, Arinzo, Angulfewa, and Orube. Dadamu Sub-county was chosen because of its long history of artisanal gold mining, which could have disturbed the deep-lying radioactive elements. In each selected cell, a khat garden was chosen, and from each, proportional numbers of soil and khat samples were collected based on the garden size.

CHAPTER TWO: LITERATURE REVIEW

2.1 Introduction

The review of the related literature covered natural radioactivity and its sources, the migration of ^{40}K, ^{232}Th, and ^{226}Ra from soil to plants and their uses, and khat and its recreational uses. The chapter further covered various ways of exposure to natural radionuclides and their health impacts on the human body. In addition, the radiation toolbox software for organ dose quantification, a high-purity germanium detector, and sodium iodide for radionuclide concentration determination were discussed. Finally, the chapter looked at similar studies on radioactivity concentrations and their findings.

2.2 Sources of radioactivity

Chemical elements are made of atoms, which in turn constitute matter. Atoms with fewer or more than eight valence electrons are said to be unstable, while stable atoms have exactly eight valence electrons in their outermost shells. Unstable atoms, which may exist in nature or be artificial, are described as 'radioactive' and undergo spontaneous decay to attain a stable state(Luis & Orcid, 2024). The decay process leads to the emission alpha particles (α), beta particles (β), and extremely penetrating gamma rays (γ), accompanied by the release of energy. Alpha radiation consists of helium nuclei composed two protons and two neutrons, resulting in a positive charged (Luis et al., 2024). They have the highest ionising potential but the least penetrating power. Beta particles are electrons, with slightly greater penetrating ability than α-particles but less ionising than α-particles. Gamma rays are electromagnetic, with a powerful penetrating potential owing to their extremely

short wavelength, but possess the weakest ionising ability. Gamma rays are deflected by neither field (electric or magnetic) due to their chemical neutrality.

Induced radioactivity involves the application of radiation to raise stable materials to an excited state, making them radioactive. In practice, major lightweight elements such as aluminium, boron, magnesium, iodine, manganese, sodium, cobalt, and caesium are the ones that can easily be excited by neutron bombardment to produce artificial radioactivity. Artificial radioactivity has applications in various fields, such as medicine for the diagnosis and treatment of diseases, industry for radioactive tracing, and for monitoring the thickness of metal sheets and paper. Other applications include manufacturing nuclear weapons, inducing mutations in plants and animals, and tracking the uptake of phosphorus by plants (UNSCEAR, 2000).

Natural radioactivity, however, involves the radioactive decay of the primordial radioactive materials that occur naturally and are found in large amounts in the Earth's crust. Terrestrial radiation and cosmic radiation are the main sources of natural radioactivity. The outer surface of the Earth's atmosphere is constantly exposed to cosmic radiation. Cosmic rays mainly consist of energetic particles from space, including electrons and protons, along with high-frequency electromagnetic radiation like gamma rays and X-rays. Their relative compositions are such that hydrogen nuclei constitute more than 85%, helium nuclei (α-particles) constitute 12%, and heavier nuclei 1%, while the electrons constitute 2% (Singh et al., 2020). These subatomic energetic particles constantly bombard the outer surface of the Earth's atmosphere and consequently get absorbed by the human body after penetrating the atmosphere. Cosmic radiation comes from multiple sources, such as the sun and celestial bodies beyond the solar system, especially

the Milky Way Galaxy and the space between galaxies. Interaction of these energetic particles with the atmosphere has been reported to cause depletion of the ozone layer, which directly influences climatic conditions and contributes to global warming (Paleari et al., 2022). Another effect of the collision of cosmic rays with the Earth's atmosphere is the production of cosmogenic radionuclides. Notable examples of cosmogenic radionuclides include carbon-14 (^{14}C), Silicon-32 (^{32}Si), chlorine-36 (^{36}Cl), aluminium-26 (^{26}Al), and sodium-22 (^{22}Na).

Terrestrial radiation, another critical source of natural radioactivity, arises from primordial radionuclides embedded in the Earth. The ^{40}K and the decay series of ^{238}U and ^{232}Th constitute the key naturally occurring radioactive elements within our environment (Olagbaju et al., 2021). These radionuclides are referred to as 'primordial radionuclides' because they existed during Earth's formation about 4.5 $\times 10^9$ years ago. Extremely long half-lives characterise them: ^{238}U, ^{40}K, and ^{232}Th have half-lives of 4.5 billion, 1.25 billion, and 14 billion years, respectively.

2.3 Radioactive decay

These radionuclides are unstable and undergo a series of successive disintegrations to attain stable isotopes. The decay series of uranium begins with ^{238}U decaying to the unstable isotope thorium-234 (^{234}Th) via alpha decay. Thorium-234 then undergoes a series of successive beta and alpha decays until a stable lead-206 (^{206}Pb) is attained. The decay series of thorium, however, begins with ^{232}Th transforming into radium-228 (^{228}Ra) after an alpha decay. Afterwards, several beta and alpha decays followed until a stable lead-208 (^{208}Pb) was produced. The decay series of ^{232}Th and ^{238}U is shown in Figure 2.1.

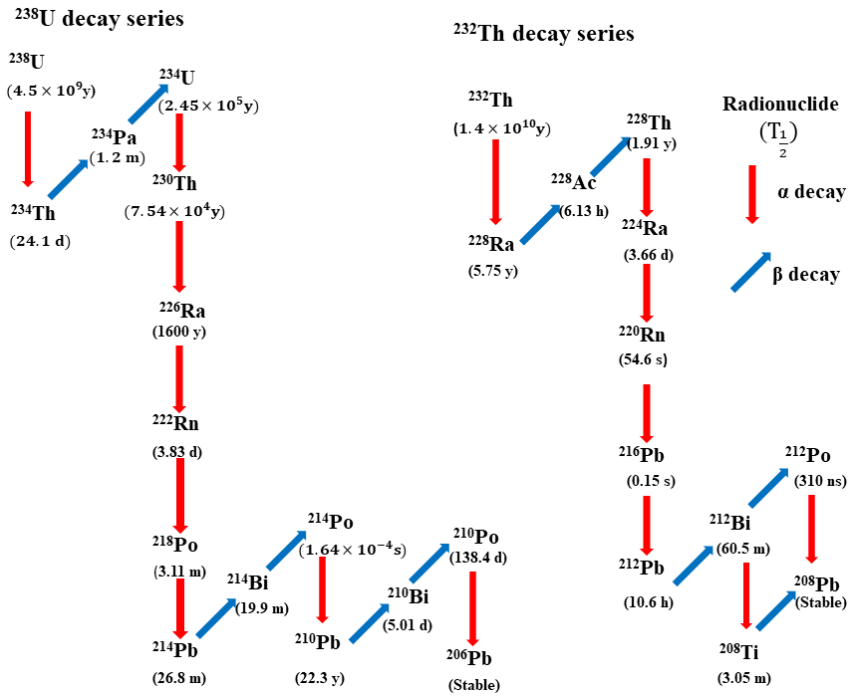


Figure 2.1: The decay chain of Radionuclides of ^{238}U and ^{232}Th (Pervin et al., 2022)**.**

It is worth noting that, as ^{238}U struggles to attain stability, radon-222 (^{222}Rn) is produced. Radon is a gas with three main forms: Radon-222 (radon), Radon-220 (thoron), and Radon-219 (actinon) as members of the decay series of ^{238}U, ^{232}Th, and Uranium-235 (^{235}U), respectively. ^{222}Rn has its origin in the radioactive decay of Radium-226 (^{226}Ra), a member of the decay series of ^{238}U. ^{222}Rn is a radioactive noble gas without taste, smell, or colour. It is produced by the spontaneous decay of ^{238}U, which is abundant in rocks, soil, and groundwater (Pervin et al., 2022). According to UNSCEAR (2000), the mean effective annual dose per person from natural radiation in the surrounding area is 2.4 mSv, of which about half is from ^{222}Rn (Ullah et al., 2022). Special attention has been drawn to 222Rn because it is responsible for most radiation hazards, with a very long half-life of 3.825 days (Ullah et al., 2022), compared to ^{220}Rn (55.6 s) and ^{219}Rn (3.96 s).

The transformation of all these unstable nuclides into stable states follows the statistical law of chance. The law of decay states that the rate at which unstable

atoms decay every second is proportional to the number of atoms remaining at that moment. The law can be summarised into the first-order linear differential Equation (2.1):

$$\frac{dN}{dt} = -\lambda t \ , \qquad (2.1)$$

where N denotes the number of atoms present after decaying for time t, while $\boldsymbol{\lambda}$ is the constant of proportionality called the decay constant, the constant $\boldsymbol{\lambda}$ represents the likelihood of an atom disintegrating in the next second. The negative sign in the equation shows that N decreases gradually as t increases. When this equation is solved by separating the variables and integrating both sides with respect to the variables, it yields Equation (2.2):

$$N = N_o e^{-\lambda t} \ , \qquad (2.2)$$

where N_o represents the number of atoms initially available when $t = 0$, and N retains its meaning as defined in section (2.1).

At half-life ($T_{\frac{1}{2}}$), the number of atoms present is half the initial value at $t = 0$. Inserting the condition above in equation (2.2) and then simplifying yields Equation (2.3).

$$T_{\frac{1}{2}} = \frac{\ln 2}{\lambda} \qquad (2.3)$$

2.4 Khat

Khat is a small, flowering plant whose leaves and stems are intentionally chewed for their stimulant effects (Al-jalali & Shaltout, 2014). The plant is known by a series of names depending on the country, such as miraa (Kenya), khat (Ethiopia),

and Mayirungi (Uganda). A vast majority of climates and soils support khat growth. The seedless plant has adapted to blossom in high-altitude and less fertile areas where many plants have failed to flourish. Khat is planted in a staggered manner for continuous supply. To retain its freshness, the harvested parts (leaves and stems) are wrapped in large banana leaves and tied in bundles (Asfaw, 2023). The bitter and sour taste of the leaves, coupled with an aromatic odour, makes it pleasant to chew. The stems and soft leaves are chewed to induce a mild feeling of excitement and euphoria. Some perpetual khat consumers make juice from dried leaves and drink it, while others smoke the dried leaves, just like tobacco (Wabe, 2011). However, it was found that drying the leaves typically leads to a significant drop in the bioactive component, and hence, fresh leaves were preferred.

Khat made its way to Uganda during colonial times and was generally sold in small amounts and consumed by Somali and Yemeni people in business (Storer et al., 2022). Khat production and consumption gained momentum nationwide, including in Arua district, in the late 1970s, and became an agricultural bandwagon in 2000 (Storer et al., 2022). Currently, the prevalence of khat production in Arua and Maracha districts stands at 80% due to its resistance to harsh conditions and year-round harvest (Storer et al., 2022). Because each person chews khat for reasons best known to him, there is scant data on the amount of khat consumed in Arua district.

Globally, khat consumption has been embraced by the majority of adults, though it is considered a form of drug abuse in some countries. For example, in Ethiopia, an average of 38% of adults reportedly chew khat daily (Teni et al., 2015). Consumption of khat is increasingly common among the youth in East Africa and the Arabian Peninsula, with over 10 million people chewing it daily (Asfaw, 2023).

Chewing is primarily done in a small group of peers or members of a particular social setting. Perpetual consumers ingest khat for several reasons, such as elevating social cohesion, reducing the need for sex and food, increasing vigilance and ceremonial purposes (Asfaw, 2023). University students cite khat chewing as enhancing their mental performance, especially when preparing for examinations. Night workers and long-distance drivers chew khat to stay awake while working. Other khat chewers claim that khat is effective in supporting diabetic patients by reducing blood glucose levels, while some assert that khat chewing is an essential remedy for asthma (Asfaw, 2023).

Laboratory experiments were conducted to determine the chemical composition of khat. Several psychotropic substances, such as alkaloids, glycine, glycosides, and ascorbic acid, were found in khat (Asfaw, 2023). Although numerous chemicals have been reported in khat, contradicting reports from the World Health Organisation indicate that khat is ranked the least harmful among the group of psychoactive substances (Asfaw, 2023). Extremely high khat use is reported to have significant consequences on the health of consumers, such as wounds in the mouth, difficulties in sleeping, urinary retention, cardiac arrhythmia, and both oral and lung cancers (Silva et al., 2022). Other adverse consequences reported include irritability, emotional imbalance, and mental disorders. It is also claimed that khat chewing raises the desire for sex in females as it induces impotence in men (Asfaw, 2023). The spectrum of consequences of khat chewing reported in the various literature was independent of the quantities of radionuclides in the khat. It is therefore expected that more serious adverse consequences would result if the khat is collected from highly radiation-contaminated soil.

2.5 Migration of radionuclides from soil to plants

Natural radionelements such as ^{226}Ra, ^{232}Th, and their progenies, including ^{40}K, are found everywhere in the environment, particularly in the atmosphere and the Earth (rocks, soil, and water), at varying concentrations. The concentration, mobility, and accumulation of these radionuclides depend is a function of multiple factors, including the geological nature of the area, soil pH, diffusion, geographic location, agricultural practices, and local climatic conditions. Khat constantly gets contaminated with these radionuclides through two mechanisms: firstly, the direct route in which the radionuclides are deposited in the aerial parts of the plants, particularly the stems and the leaves and via root uptake in which plants absorb these radionuclides during mineral uptake alongside the nutrients and water from the soil (Tyovenda et al., 2022). Additionally, practices, such as applying potassium-based fertilisers to the soil, increase plants' exposure to radionuclides (Techan, 2021). This, in turn, leads to an increase in radionuclide concentration in the plants. The migration of radionuclides from radiation-contaminated soil, air, and water to plants is a worldwide concern as it determines the radiation health risks to humans and their surroundings.

2.6 Soil-to-plant transfer factor

Plants are the points of convergence for radionuclides from contaminated soil, air, or water. The quantity of radionuclides absorbed by edible plants determines the amount likely to be transferred into the human food chain. The plant uptake of radioactive materials is quantified using a parameter called the soil-to-plant transfer factor (TF). The TF is a vital tool for evaluating the consequences of accidental or recurrent spread of radionuclides into the soil and its agricultural

products. For a fixed mass of plant and soil picked from the same point, TF is the quotient comparing the activity concentration of the plant to the corresponding activity concentration of the soil. The TF values vary globally based on differences in soil types, vegetation, and environmental conditions (UNSCEAR, 2000). Practices such as irrigation, ploughing, spraying plants with pesticides, fertilization, and liming agricultural land significantly affect TF values.

2.7 Exposure to radionuclides

Exposure refers to the energy released in air by specific types of radiation, whereas dose represents the amount of energy absorbed by matter. All exposure pathways are classified as internal or external. Internal exposure takes place when the source is within the body, whereas external exposure happens when the radiation source is at some distance from the body. Examples of internal exposure are inhalation and ingestion of radioactive substances. Exposure through ingestion occurs when the radioactive materials enter the human food chain through any one of the following ways: swallowing through the mouth and absorbing via the digestive tract, absorption by the skin (percutaneous absorption), wound contamination, and intake of radioactive materials through injections or radiopharmaceuticals (Manchikanti et al., 2023).

Inhalation of airborne radioactive particles introduces them into the human body. This pathway is common with radiation-contaminated smoke, dust, and radionuclides in the gaseous phase, such as radon-222 (^{222}Rn). Once inhaled, the ^{222}Rn gas is expelled from the lung via exhalation, while its short-lived progenies, such as Polonium-218 and Polonium-214, are trapped in the lung, particularly in the bronchial epithelium lining of the lung (Azhdarpoor et al., 2021). The ^{222}Rn

progenies above emit highly ionising alpha particles, which can damage DNA and cause lung cancer. The WHO identifies ^{222}Rn as the cardinal cause of lung cancer in non-smokers, and it contributes to over 50% of the total annual radiation exposure dose (Azhdarpoor et al., 2021).

Direct exposure pathway occurs when an individual is exposed to radionuclides of natural origin, which are common in our environment. Direct exposure is an example of external exposure. These radiations can either be from outer space, such as cosmic rays, or the radioactive rocks and soil within the environment, or from the effects of nuclear bomb tests, which leave radioactive substances in the environment. Other external exposure routes include absorption of radiation from building materials, radiation generators, suspended matter, and body surface contaminations (Little et al., 2023).

2.8 Health effects due to natural radionuclide exposure

Radiation emitted by natural radionuclides is highly ionising due to its excess energy and can produce stochastic and non-stochastic effects. The degree of health hazards they cause is a function of the absorbed dose and the duration of exposure. Exposure to low levels of radiation for a long time is reported to be associated with cancer of the breast, lung, blood, and genetic mutation (Saenboonruang et al., 2018). In contrast, short-term exposure to elevated levels of radiation is associated with radiation burns and poisoning (Olagbaju et al., 2021).

^{232}Th has been reported to enter the bloodstream via inhalation, and more than 75% is deposited in organs such as the liver, lungs, and bones. At the same time, a negligible fraction is retained in the kidneys (Muller et al., 2019). Once inside the lungs, ^{232}Th particles can persist and expose tissues to radiation over time, hiking

the chance of lung cancer (Muller et al., 2019). In addition, several diseases, including respiratory complications, haematological and pulmonary disorders, congenital anomalies, and carcinogenesis, are linked to ^{232}Th contamination due to the alpha particles it emits (Muller et al., 2019).

The ^{40}K, however, is essential for several biological processes, such as the regulation of nerves, the heart, and muscles. Excessive exposure to ^{40}K leads to health-related problems, referred to as hyperkalemia, which is responsible for kidney and heart failure due to the beta particles and gamma rays they emit. (Zhang et al., 2022) reported that exposure to ^{238}U isotopes may cause chemical damage to organs such as the kidneys, gonads, lungs, liver, and skeletal system.

2.9 Gamma-ray spectroscopy

This refers to a quick, non-destructive analytical technique for detecting various radioactive elements in a given sample. During the spectroscopy, the detector measures the energy of the incoming gamma rays. This energy is unique and corresponds to only one isotope. The exact identity of the radionuclide emitting gamma rays is usually determined by matching the determined energy to the known energies of gamma rays released by the specific isotopes. The most commonly used gamma-ray detectors are scintillation and semiconductor detectors.

2.9.1 Scintillation detectors

These detectors operate based on the principle that light is produced when gamma rays interact with appropriate scintillator materials (organic or inorganic). The photomultiplier tube transforms light flashes into electrical signals through the photoelectric effect. The electrical circuit further processes these voltage pulses to provide detailed information on the gamma-ray energy spectrum. Several inorganic

scintillation materials exist, such as sodium iodide (NaI), zinc sulphide (ZnS), caesium iodide (CsI), and lithium iodide (LiI). A NaI crystal, which has a high atomic number, is preferred due to its strong stopping power (Buchtela et al., 2019). In practice, it consists of a small amount of thallium introduced into the sodium iodide crystal lattice to serve as the centre of activation and increase its luminescence. Whereas various materials can serve as solid scintillation detectors, sodium iodide crystals remained the preferred choice for gamma-ray detection due to their favourable properties and affordability. A commonly used scintillation detector is thallium-doped sodium iodide (NaI (Tl)).

2.9.2 Semiconductor detectors

The physics behind the operation of these detectors is rooted in the electron energy bands in the crystal of semiconductors. Germanium as a semiconductor has a narrow band gap of about 0.66 eV (Buchtela, 2019). When gamma rays strike the germanium crystal, a large amount of energy is absorbed, raising electrons from the occupied energy band to the free-electron band. The migration of the electron-hole pair through the semiconductor due to the electric field leads to a change in conductivity, which can be detected (Buchtela, 2019). The corresponding electrical signal indicates the passage of radiation. High-purity germanium (HPGe) and germanium crystals doped with a small amount of lithium germanium are among the most common semiconductor detectors. Detectors containing a germanium crystal generally have much greater resolution than NaI (TI). A series of peaks observed with the germanium detectors is not detected by the NaI (Tl) detector. In contrast, Ge (Li) must be kept at a temperature of -196 ℃ for the rest of its lifetime. An HPGe detector can be kept at room temperature continuously but requires a constant supply of liquid nitrogen for cooling during use (Reguigui et al., 2014).

2.10 Performance of the gamma-ray spectrometry system

Qualitative and quantitative measurements of gamma-emitting radionuclides can be performed using a gamma-ray spectrometer. The quality or the degree of accuracy of the experimental results is a function of the performance specifications of several system detectors. The key performance specifications are the detector efficiency and detector resolution. Other factors that determine the accuracy of gamma-ray analysis results include sample mass, shielding level, internal and external background levels, and the geometry used (Hafızoğlu et al., 2024). The detector's resolution defines its capacity to separate two gamma lines having similar energies. Better-resolution detectors produce spectra with narrow peaks. The design of the gamma-ray spectrometry system provides options for adjusting it to generate symmetrically sharp, high-resolution peaks. The energy of the gamma-ray determines the horizontal location of the peaks. At the same time, the detector efficiency and the gamma-ray intensity depend on the peak area.

Resolution defines the detector's capacity to separate two adjacent energy peaks. The energy resolution is determined by measuring the peak's width at the midpoint of its maximum height. The value obtained is also known as *full width at half-maximum* (*FWHM*). The lower the FWHM at a particular energy, the better the resolution. The energy resolution can be expressed as a percentage or as an absolute value in kiloelectron Volts (keV), as shown in Equation (2.4) (Hafızoğlu et al., 2024).

$$R = \frac{FWHM}{H_O} \times 100\% \ , \qquad (2.3)$$

where H_o represents the peak centroid and R represents the detector's energy resolution

Efficiency is among the key parameters used for measuring the detector's performance. Detector efficiency is classified into three types: absolute, relative, and intrinsic efficiency. All radionuclides emit gamma radiation, which is detected by appropriate detectors, such as NaI scintillators or HPGe detectors. However, the detector registers fewer photons than the actual number produced by the source. The absolute efficiency, ε, is the ratio of the total gamma radiation detected to the actual number of gamma-ray photons radiated from the source, as given in Equation (2.5) (Hafızoğlu et al., 2024).

$$\varepsilon = \frac{N_D}{N_{D_E}} \times 100\% \ , \tag{2.4}$$

where N_D represents the total gamma-ray photons detected, while N_E represents the actual number of gamma-ray photons the source emits.

Absolute efficiency allows gamma radiation of a definite energy to pass through the detector, interact with the semiconductor crystals, and be detected. Relative efficiency measures the performance of the HPGe detector relative to a 3 × 3-Inch (7.5×7.5 cm) Sodium Iodide (NaI) crystal when a 25 cm separation exists between the source and the detector crystal. At the same time, the photon energy is 1.33 MeV (Reguigui, 2014). Intrinsic efficiency represents the proportion of photons detected to the number of photons striking the detector surface. This efficiency plays a lesser role in determining the activity of a radioactive source, but it helps in comparing two or more detectors.

2.11 Related studies about the radioactivity concentration in soil and khat

The increased levels of radioactive elements in soil and khat have been a worldwide concern for several decades. Many plants with therapeutic properties

are available among community members, but contamination of the soil with radioactive substances has rendered them impure and partially unsafe for consumption. This work has included some related research findings from other researchers worldwide.

A study by Ngari et al (Njagi et al., 2022) on khat and soil samples from Embu County in Kenya revealed the average activity concentrations of 875.8 ± 11.0 Bq kg^{-1} for ^{40}K, 10.1 ± 1 Bq kg^{-1} for ^{238}U, and 51.1 ± 4 Bq kg^{-1} for ^{232}Th in khat. The average activity concentrations in soil for ^{232}Th, ^{238}U, and ^{40}K were 33 ± 5, 22 ± 11, and 344 ± 12 Bq kg^{-1}, respectively. The radiological hazards were evaluated by considering parameters like the absorbed dose rates in soil, the $ACED_{Ing}$, internal and external hazard indices, excess lifetime cancer risk, and gamma index. All the estimated hazard parameters were below their respective worldwide averages and posed insignificant health threats.

A study by Techan et al (Techan, 2021) on the assessment and investigation of the levels of natural radioactivity in soil and khat from Haramaya, Ethiopia. The average activity levels of ^{40}K, ^{226}Ra, and ^{232}Th in soil were 794.10 ± 26.44, 23.72 ± 0.85, and 111.50 ± 4.21 Bq kg^{-1}, respectively. The mean activities of ^{232}Th and ^{40}K were above the world's permissible limits, while that of ^{226}Ra was below the world's permissible limit. The study evaluated various radiological hazard parameters in soil and found that the values were below their respective world-permissible limits. The corresponding average activity levels of ^{226}Ra, ^{232}Th, and ^{40}K in khat were 1.32 ± 0.24, 10.36 ± 0.96, and 237.79 ± 7.39 Bq kg^{-1}, respectively, of which all were below the world's permissible limits. However, the average annual effective dose of khat was eight times higher than the world's permissible limit.

CHAPTER THREE: MATERIALS AND METHODS

3.1 Introduction

This chapter highlighted the study area's location and geology. Major economic activities, a detailed description of the sample collections and preparations, and a detailed description of how the gamma-ray spectrometer system, coupled with an HPGe detector, was set up. The chapter further presented how the calibrations (for energy & efficiency) were performed, including the background measurements. Chronological computations of activity concentrations and the key radiological hazard parameters, the transfer factors, and the organ doses from the measured activities were also reviewed.

3.2 Study Area

Dadamu sub-county spans an area of 33.78 km^2 on an extended stretch of land and has an approximate population of 48,100 people (Uganda Investment Authority, 2021). The major economic activities in Dadamu Sub-county include fishing along the shore of the River Nile and agriculture, producing khat as the main cash crop. Dadamu sub-county lies between latitudes $3^o\ 02'18.3''$ N and $30^o\ 59'05.7''E$. Dadamu sub-county has several streams such as Anyau and Iriova, which flows through it, depositing alluvial gold within its environment. The existence of alluvial gold and the subsequent mining activity in Dadamu sub-county dates back in 1960 (Taylor et al., 2014). Additionally, according to the geological surveys, Arua district has been reported to contain uranium ore deposits and gold (International & Agency, 2023). Dadamu sub-county is one of the notable locations in the Arua district where small-scale artisanal gold mining occurs. Local miners typically extract gold from alluvial deposits along the rivers and stream beds.

During the gold mining process, radioactive elements may be unearthed, particularly if the gold is found in geological formations that contain radioactive materials (Odumo et al., 2011). Recently, mining activities have been suspended or halted in most mining areas in Uganda, including Dadamu Sub-county. This was due to unlicensed operations and illicit activities affecting the environment. However, the unearthed radioactive elements continue to contaminate the soil and the plants they support. Therefore, there is a need to investigate the extent of contamination of soil and khat in the Dadamu Sub-county, as well as the potential health risks they pose to humans. The locations of the sample collection points are shown in Figure 3.1(a)-(c).

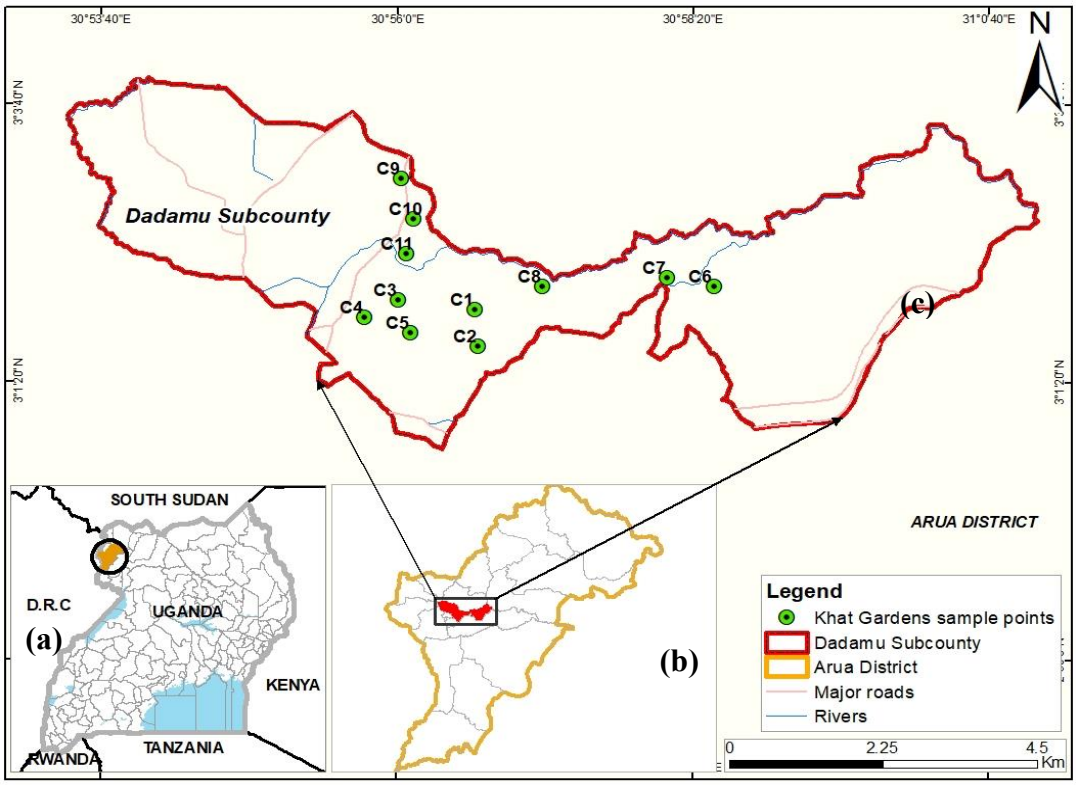


Figure 3.1: (a) Map of Uganda, (b) Arua District, and (c) Sample collection points in Dadamu sub-county.

3.3 Sample collection

Eleven khat samples were collected from five randomly selected locations in Dadamu Sub-county. From each location, 1 to 3 samples were collected, depending on the garden size. The breakdown of the number of samples per garden is shown in Table 3.1. Before sample collection, the khat garden at each location was partitioned into multiple squares measuring 10 m, and each square served as a sampling point (International Atomic Energy Agency, 2019). For each sampling point, approximately 1.5 kg of fresh khat leaves were collected from at least five randomly selected khat plants. The khat leaves from the selected khat plants were then mixed to form a composite sample and stored in a plastic bag marked with the sampling point code.

Similarly, eleven soil samples were collected at each collection point where khat was obtained. At each sampling point, the uppermost soil layer around the khat plant was cleared of pebbles and other foreign material. For each khat plant considered, a 200 g portion of soil was gathered from around the plant at a depth of 20 cm using a soil sampler (see Figure 3.2). The soil samples were thoroughly homogenised to create a composite sample (International Atomic Energy Agency, 2019). The composite samples were kept in labelled plastic bags and safely delivered to the laboratory for processing.

Table 3.1: Sample collection matrix per location.

Location	Number of soil samples	Number of khat samples	Total
Ndriba cell	2	2	4
Orube cell	3	3	6
Arinzo	3	3	6
Angulfewa	1	1	2
Ariwara	2	2	4
Total	11	11	22

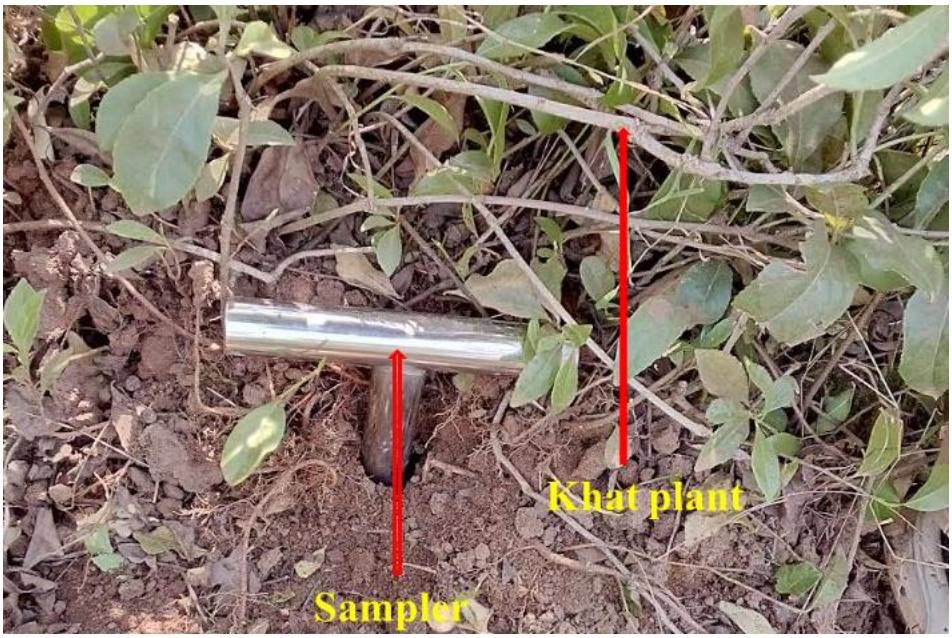


Figure 3.2: Soil sample collection using a sampler.

The coordinates of each sampling point were recorded from the centre of the square area using a handheld Garmin 64S global positioning system (GPS). The GPS coordinates of the sampling locations are displayed in Table 3.2. Sample codes were used to track and trace each sample's origin. For example, C1 and C2

represent sampling points from the Ndriba cell, and C3 to C5 represent sampling points from the Orube cell (see Table 3.2).

Table 3.2: The GPS coordinates of the sampling points**.**

Locations	Sample codes	Latitude (N)	Longitude (E)	Elevation (m)
Ndriba cell	C1	03° 01.9081′	030° 56.4233′	1161
	C2	03° 01.9031′	030° 56.4334′	1176
Orube Cell	C3	03° 01.7900′	030° 55.9793′	1199
	C4	03° 01.7785′	030° 55.7934′	1201
	C5	03° 01.7716′	030° 55.7950′	1200
Arinzo cell	C6	03° 02.1418′	030° 58.4998′	1096
	C7	03° 02.1478′	030° 58.4776′	1098
	C8	03° 02.1379′	030° 58.1476′	1099
Angulfewa	C9	03° 03.0384′	030° 56.0049′	1163
Ariwara	C10	03° 02.5787′	030° 56.0944′	1152
	C11	03° 02.5655′	030° 56.0897′	1154

3.4 Sample preparation

The picked samples were taken to the laboratory for processing. The khat leaves were thoroughly rinsed with clean tap water to eliminate dust particles. The leaves were then sliced into smaller sections with a knife and left to dry in the air for 24 hours. The samples were again dried in an electric oven at about 115 ℃. The dried sample was milled into fine powders using an electrically powered stainless-steel grinder shown in Figure 3.3(b). The powder khat samples were then placed on small aluminium disks (See Figure 3.3a) and further oven-dried at about 115 ℃ while their masses were monitored. The drying of the samples ceased when the change in mass became insignificant (Techan, 2021). The powdered khat was

passed through a 2 mm diameter sieve in order to achieve a uniform particle size distribution. After sieving, about 200 g of fine powder was obtained from each sample. The powder samples were packed in Marinelli beakers, securely sealed with masking tape as illustrated in Figure 3.4 and kept at 25 ℃ for 28 to 35 days to attain radioactive secular equilibrium between ^{226}Ra, ^{222}Rn, and their progenies (Turyahabwa, 2024).

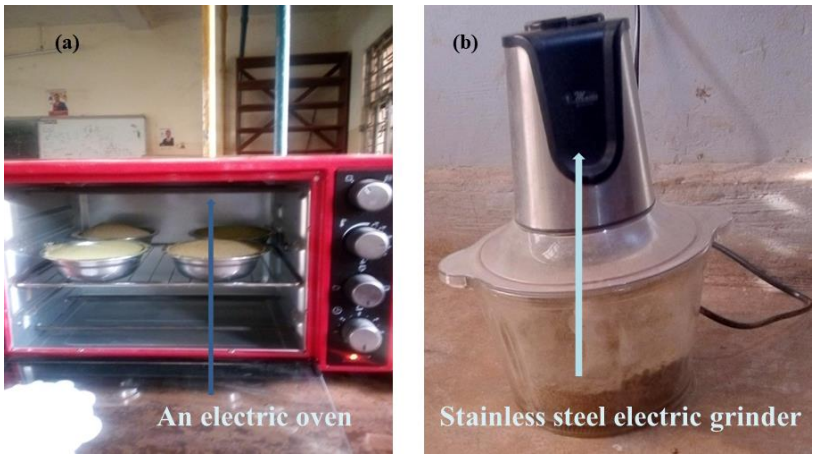


Figure 3.3: (a) Powder khat samples in aluminium disks placed in an electric oven, and (b) a stainless steel electric grinder for grinding the soil and khat samples.

The soil samples, placed in metallic trays, were air-dried for 24 hours, then oven-dried at 115 ℃ for a minimum of 4 hours to eliminate moisture and attain a stable mass. The perfectly dried samples were finely milled into powder and passed through a 2 mm sieve. The milled soil samples (about 200 g) were then packed into Marinelli beakers, sealed with masking tape as shown in Figure 3.4, and kept in the laboratory for the same period as the khat samples.



Figure 3.4: The prepared samples of soil and khat are placed in separate rows, ready for analysis.

3.5 Gamma-ray spectrometry system setup

The gamma-ray spectrometer that was used for the analysis had the following components; a high-purity germanium (HPGe) semiconductor detector, liquid nitrogen in a 35 L Dewar vessel used as a cooling liquid, analog-to-digital converter (ADC), high voltage power supply, preamplifier, linear amplifier, computer-based software for data acquisition and analysis (Genie 2000), and a multichannel analyzer (MCA). The spectrometer system's modern design integrated the high-power supply, an amplifier, an ADC, and a multichannel analyser into a single box. The components were connected as shown in Figure 3.5.



Figure 3.5: The setup of HPGe detector components used to analyse the samples.

The detector used was an n-type coaxial model manufactured by Canberra Industries (USA), with a relative efficiency of 20% and an energy resolution of 1.80 keV (FWHM) at the 1332.5 keV energy peak of cobalt-60 (^{60}Co). The MCA model 1331, serial number 13000063, from Canberra Industries was used for the analysis. The computer controlled the switching on and off of the high-voltage supply to the detector through the interface software. To minimize thermal excitation of electrons within the detector, which may interfere with gamma-ray detection, the detector was operated at liquid nitrogen temperature (-196℃). The detector was shielded from environmental photon sources by a rectangular enclosure made of Lead blocks, each 10 cm thick. Lead was selected for its ability to absorb radiation with different levels of penetrating power.

3.5.1 Energy calibration

To identify the radionuclide emitting gamma rays, the energy calibration was performed using a mixed standard containing Cobalt-60 (60Co) and Caesium-137 (137Cs), certified by the Uganda Atomic Energy Council. Cobalt-60 and caesium-137 were chosen because they emit gamma rays at known energies of 1332.5 keV and 662 keV, respectively. The standard sources were placed on the lead-shielded HPGe detector and counted until a sufficient number of counts was obtained to clearly define the energy peaks. The MCA produced a linear correlation between the gamma-ray energy and the centroid channel number, as illustrated in Figure 3.6. The calibration process was performed using channel numbers 1024 to 8192, with a step size of 1024. The linear relationship between the energy and the channel numbers is the MCA-generated energy calibration line, having the gradient 0.2606 keV ch^{-1} and is given by Equation (3.1):

$$E(keV) = 0.2606 \times Ch + 0.4907 \quad (3.1)$$

In gamma-ray spectrometry with an HPGe detector, the channel number representing the detector signal pulse is directly proportional to the energy deposited, yielding a linear relationship.

The significance of this equation is that, for any specific channel number *Ch* on the MCA, the corresponding energy *E* can be determined by inputting that channel number.

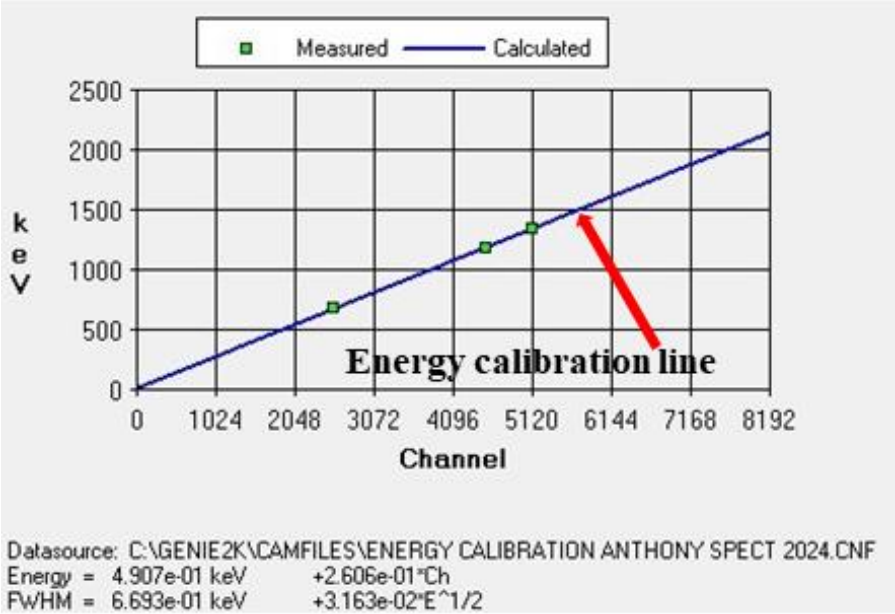


Figure 3.6: The energy calibration graph produced by the Genie-2000 software.

3.5.2 Efficiency calibration

Efficiency calibration in gamma-ray spectrometry is performed to accurately determine the relationship between the detected gamma-ray counts and the actual radiation emitted by the source. This process is vital because the detector efficiency varies with gamma-ray energy, geometry, and sample positioning. Knowing the detector's efficiency at different energies allows the activity concentrations of the radionuclides in the samples to be accurately measured. In this study, efficiency calibration was executed using a mixture of standard samples of Cobalt-60 (^{60}Co)

and Caesium-137 (^{137}Cs) certified by the Uganda Atomic Energy Council. Using the set of pairs of efficiency and gamma-ray energy computed by the Genie 2000 software, with energies ranging from 0 to 2500 keV, the efficiency calibration curve shown in Figure 3.7 was obtained.

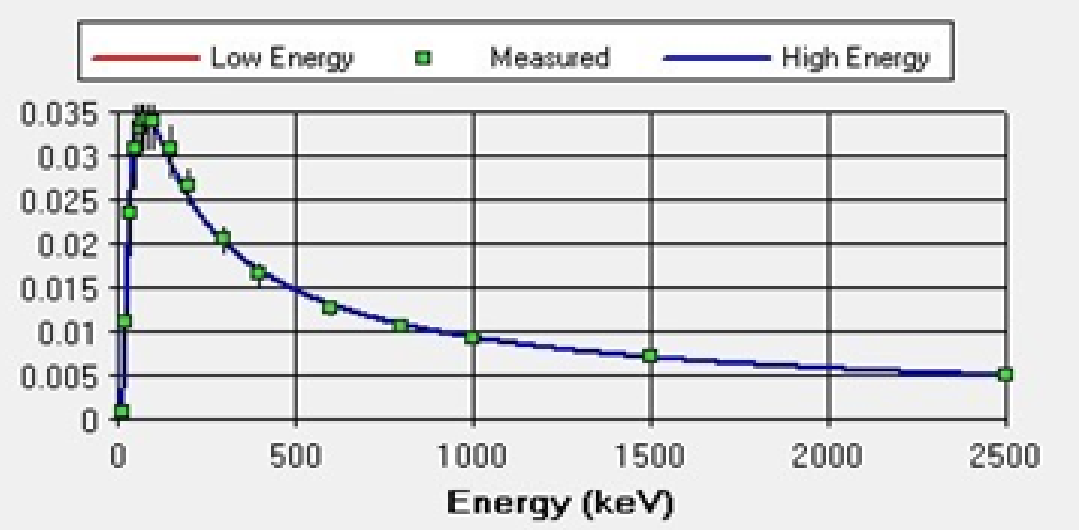


Figure 3.7: The efficiency calibration curve for the HPGe detector used to calculate the activity concentrations of ^{232}Th, ^{40}K, and ^{226}Ra in the samples.

3.5.3 Background radiation count

To account for gamma-ray photons originating from sources other than the prepared samples, the background count was measured by placing an empty Marinelli beaker on the lead-shielded detector and counting for 21,600 s. The background count was subsequently subtracted from the measured count rates for each sample to obtain the net counts.

3.5.4 Determination of the activity concentrations of the radionuclides

After approximately one month of storage, the samples were presented for analysis. The specifications of the measuring instruments are stated in Section 3.5. Each soil and khat sample was placed on the detector cavity, which is highly shielded with

lead blocks of thickness 10 cm. The count for each sample was measured for 21,600 s, as was the background. The activity concentrations of each radionuclide were calculated based on the weighted averages of its progenies at defined energies. For example, the ^{226}Ra activity concentration was calculated from its progenies, ^{214}Pb and ^{214}Bi, at the energies shown in Table 3.3. The ^{232}Th activity concentration was determined from the weighted averages of the progenies ^{212}Pb and ^{228}Ac at energies shown in Table 3.3. In contrast, the activity concentration of ^{40}K was determined from its discrete gamma emission line at 1460.8 keV. The branching ratios (Column 4 of Table 3.3) are essential in calculating the activity concentrations because they represent the probability that a particular nuclear decay will emit gamma radiation at a specific energy.

Table 3.3: Gamma-ray lines and their corresponding branching ratios used in calculating the activity levels of ^{232}Th, ^{40}K, and ^{226}Ra.

Radionuclide	**Detected progeny**	**Energies used (keV)**	**Branching ratio (%)**
^{226}Ra	^{214}Pb	295.2	19.2
		351.9	37.2
	^{214}Bi	609.3	46.3
^{232}Th	^{212}Pb	238.6	44.6
	^{228}Ac	911.6	27.27
		969.1	16.6
^{40}K	^{40}K	1460.8	10.7

The activity concentrations of the specific radioelements in soil and khat were calculated from background-corrected radionuclide counts at particular energy levels using Equation (3.2) (Biira et al., 2021).

$$A_C = \frac{N_C}{P_\gamma \times t \times m \times \varepsilon} \quad , \tag{3.2}$$

where A_c is the activity concentration in Bq kg^{-1}, Nc is the background-adjusted count, P_γ is the absolute gamma emission transition probability, $\boldsymbol{\varepsilon}$ is the detector efficiency, m represents the sample mass in kg, and t is the duration of counting in seconds.

3.6 Soil-to-plant transfer factor

Mathematically, the transfer factor values are computed from Equation (3.3) (Ugbede et al., 2021)

$$TF = \frac{A_P}{A_S} \, , \tag{3.3}$$

where A_p represents the activity concentration of radionuclides in the dry weight of the plant and A_s denotes the specific activity of radionuclides in the dry weight of the soil, all measured in Bq kg^{-1}.

3.7 Radiological hazard parameters

To evaluate the radioactivity-related hazards emanating from soil and khat, the following parameters were employed: the radium equivalent activity, the absorbed gamma dose rate, the yearly effective equivalent (indoor and outdoor), the annual effective ingestion dose of khat, and excess lifetime cancer risk.

3.7.1 Radium equivalent activity

Radium equivalent activity (Ra_{eq}) is a useful parameter for comparing the activity levels in different samples, especially when dealing with non-uniform distributions of the radionuclides. The overall radiological hazard posed by the samples can be quantified using Ra_{eq}, which provides a single value that accounts for radionuclide concentrations such as ^{232}Th, ^{226}Rn, and ^{40}K. When computing Ra_{eq}, 1 Bq kg^{-1} of ^{226}Ra was treated as the baseline value (UNSCEAR, 2000). Similarly, 1 Bq kg^{-1} of ^{232}Th was assumed to yield 1.43 times the gamma dose of 1 Bq kg^{-1} of ^{226}Ra, while 1 Bq kg^{-1} of ^{40}K was assumed to produce 0.077 times the gamma dose of ^{226}Ra. The Ra_{eq} value was computed using Equation 3.4 (Ugbede et al., 2021) because 4,810 Bq kg^{-1} of ^{40}K, 370 Bq kg^{-1} of ^{226}Ra, and 259 Bq kg^{-1} of ^{232}Th yield identical gamma-radiation dose effects.

$$Ra_{eq} = A_{Ra} + 1.43A_{Th} + 0.077A_K \ , \qquad (3.4)$$

where A_{Th}, A_K, and A_{Ra} represent the activity concentrations of ^{232}Th, ^{40}K, and ^{226}Ra, respectively.

3.7.2 Absorbed gamma dose rate

The absorbed dose rate (D_R) defines the quantity of energy deposited by gamma radiation in 1kg of matter (usually air or tissue) per unit time, measured in (J/kg). These gamma radiations are emitted by ^{232}Th, ^{226}Ra, and ^{40}K. The D_R values for each sample were calculated from the radionuclide activity concentrations using Equation (3.5) (Ugbede et al., 2021).

$$D_R\left(nGyh^{-1}\right) = 0.462A_{RA} + 0.604A_{Th} + 0.0417A_K \ , \qquad (3.5)$$

where 0.604, 0.0417, and 0.462 represent the dose conversion factors of ^{232}Th, ^{40}K, and ^{226}Ra, respectively. These conversion factors transform activity concentrations into dose rates ($\mathrm{nGyh^{-1}}$ per $\mathrm{Bq\ kg^{-1}}$) (Ugbede et al., 2021).

3.7.3 Annual effective equivalent dose

This parameter estimates the risks of exposure to ionising radiation (from indoor Ein and outdoor Eout) within a year. The annual effective dose equivalent is used to assess the biological effects of different types of radiation on human tissues. An assumption that people spend 20% of a day (24 hours) outside their dwellings and 80% of a day inside was used to compute the dose (Ugbede et al., 2021). The annual effective equivalent doses are derived from absorbed dose rates using 0.7 $\mathrm{SvGy^{-1}}$ to convert absorbed dose rates in air to the effective dose received by adults. Equations (3.6) and (3.7) were used to calculate the annual doses (Kanayochukwu et al., 2022). The factor 10^{-6} was used to convert nanosieverts to millisieverts

$$E_{out}\left(mSvy^{-1}\right) = D_R\left(nGyh^{-1}\right) \times 8760 \times 0.2 \times 0.7 \times 10^{-6}\ , \tag{3.6}$$

$$E_{in}\left(mSvy^{-1}\right) = D_R\left(nGyh^{-1}\right) \times 8760 \times 0.8 \times 0.7 \times 10^{-6}\ , \tag{3.7}$$

3.7.4 Annual committed effective ingestion dose from khat

The quantity of ionising radiation an individual receives annually by consuming radioactive materials in khat represents the annual effective ingestion dose. It is part of internal radiation exposure through khat chewing and was derived from the activity concentrations of the respective radionuclides using Equation (3.8) (Kanayochukwu et al., 2022).

$$ACED_{ing} = A_C \times D_C \times IR_{ing}\ , \tag{3.8}$$

Where, $ACED_{ing}$ is the annual effective ingestion dose, A_c is the activity of each radionuclide in khat, IR_{ing} represents the amount of khat consumed annually, given by Equation (3.9) (Techan, 2021).

$$IR_{ing} = \text{Khat ingested (kg d}^{-1}) \times 365 \text{ days}, \quad (3.9)$$

where D_c represents the dose coefficient for the ingestion of radionuclides by adults. The values of D_c in (mSv Bq^{-1}) used were 2.3×10^{-4} $SvBq^{-1}$, 6.2×10^{-6} $SvBq^{-1}$, and 2.8×10^{-4} $SvBq^{-1}$ for ^{232}Th, ^{40}K, and ^{226}Ra, respectively (Abojassim et al., 2014). A 0.5 kg per day consumption rate was used as reported in (Abojassim et al., 2014).

3.7.5 Excess lifetime cancer risk

The excess lifetime cancer risk (ELCR) refers to the likelihood of an individual developing cancer over their lifetime due to internal exposure arising from khat chewing. The ELCR value depends on the dose of carcinogens absorbed. The excess lifetime cancer risk was derived from the $ACED_{ing}$ of khat and was calculated using Equation (3.10) (Kolapo & Oluwatosin, 2018).

$$ELCR = ACED_{ing}\left(mSvy^{-1}\right) \times RF\left(Sv^{-1}\right) \times DL \times 10^{-3}\ , \quad (3.10)$$

where $ACED_{ing}$ represents the annual effective dose from khat ingestion, *RF* is the risk factor of radiation-induced fatal cancer per Sievert, taken as 0.05, and *DL* is the life expectancy. A duration of 64 years was chosen to represent Ugandan life expectancy, based on data from the Uganda Bureau of Statistics (UBOS) (UBOS, 2024).

However, the potential carcinogenic effects arising from soil and other construction materials were calculated using Equation (3.11) (Ugbede et al., 2021).

$$ELCR = E_{out}\left(mSvy^{-1}\right) \times RF\left(Sv^{-1}\right) \times DL \times 10^{-3} \ , \qquad (3.11)$$

where E_{out} represents the total annual effective dose equivalent from outdoor exposure computed in section 3.6.3.

CHAPTER FOUR: RESULTS AND DISCUSSIONS

4.1 Introduction

This chapter presents the study results in tabular and graphical forms. The results include the activity concentrations of the radioactive elements in soil and khat, the transfer factors, and the major radiological hazards. The radiological hazard parameters considered were the radium equivalent activity, absorbed dose rate, annual committed effective dose equivalent, and ELCR. The annual organ doses generated by the Rad Toolbox software for 15 selected body organs were also presented and analysed.

4.2 Activity concentrations

4.2.1 Soil samples

Table 4.1 shows ^{232}Th, ^{40}K, and ^{226}Ra activity levels of radioelements in each soil and khat sample. For soil, the mean activity concentration of ^{226}Ra was 23.32 ± 5.59 Bq kg^{-1}, which was 33% below the world permissible limit of 35 Bq kg^{-1}. Calculated average activity concentrations of ^{232}Th and ^{40}K were 59.16 ± 13.55 and 512.05 ± 149.27 Bq kg^{-1}, respectively. According to UNSCEAR, the global permissible limits for the activity levels of ^{232}Th and ^{40}K were 30 and 400 Bq kg^{-1}, respectively (UNSCEAR, 2000). However, it should be noted that the mean activities of ^{232}Th and ^{40}K exceeded the global permissible limits by 97% and 28%, respectively. This implies that continuous use of the agricultural soil for khat production can increase radiation exposure and its associated health risks.

As shown in Table 4.1, ^{40}K exhibited the highest average concentration, followed by ^{232}Th and ^{226}Ra. The high levels of ^{40}K in the soil can be attributed to multiple factors, including geological origins and human activities. From a geological

perspective, gold deposits usually occur in feldspar-rich rocks, especially potassium feldspar and biotite mica, which contain a large amount of ^{40}K (Zhakypbek et al., 2025). When these rocks are broken down, K^+ is released into the soil, thereby increasing the soil's ^{40}K content. Additionally, mining activities could have exposed mine tailings to the surface, thereby accelerating the release of ^{40}K into the environment. The increased levels of ^{40}K in the soil may be associated with agricultural practices, such as the use of potassium-rich fertilisers and pesticides on cultivated land to boost khat production in the region. Generally, the findings revealed that the mean concentration of the radionuclides in soil follows the order $^{40}K > ^{232}Th > ^{226}Ra$, which aligns perfectly with study findings reported in Ethiopia (Techan, 2021) and Kenya (Njagi et al., 2022).

Table 4.1: Activity concentrations of ^{232}Th, ^{40}K, and ^{226}Ra in soil from the Dadamu sub-county.

Sample codes	Activity concentration in soil (Bq kg^{-1})		
	^{226}Ra	^{232}Th	^{40}K
C1	23.38 ± 3.47	110.05 ± 8.83	607.85 ± 14.56
C2	16.04 ± 2.33	99.64 ± 8.82	564.98 ± 12.52
C3	17.94 ± 0.60	27.71 ± 0.51	206.04 ± 14.12
C4	13.36 ± 0.10	25.33 ± 0.03	71.40 ± 18.20
C5	3.56 ± 0.03	8.85 ± 0.20	106.50 ± 6.14
C6	75.84 ± 1.41	152.97 ± 0.64	1883.13 ± 49.48
C7	23.64 ± 0.10	39.45 ± 4.71	649.17 ± 9.38
C8	22.77 ± 2.65	56.31 ± 2.91	500.37 ± 24.04
C9	13.25 ± 1.81	13.64± 6.61	393.58 ± 11.25
C10	22.61 ± 3.56	63.25 ± 3.80	367.46 ± 2.78
C11	24.10 ± 2.75	53.52 ± 3.50	282.07 ± 23.98
Ave	23.32 ±5.59	59.16 ±13.55	512.05 ± 149.27
Min	3.56 ± 0.03	8.85 ±0.20	71.4 ±18.20
Max	75.84 ±1.41	152.97 ±0.64	1883.13 ±49.48

2.2 Khat samples

For khat, the estimated activity levels of ^{232}Th, ^{40}K, and ^{226}Ra are shown in Table 4.2. The average ^{226}Ra activity concentration was 7.24 ± 1.56 Bq kg^{-1} which was 79% below the global permissible limit. The average ^{232}Th activity concentration recorded was 5.60 ± 1.39 Bq kg^{-1} , which is 81% below the globally accepted safety limit. The ^{40}K average activity level was 322.92 ± 72.22 Bq kg^{-1} which negatively deviates from the globally accepted safety limit 19. In general, the activity concentrations recorded in khat were below the recommended safe limits and pose no significant health threat to humans.

In a comparison of the ^{232}Th, ^{40}K, and ^{226}Ra activity concentrations in khat samples, it is noted that the activity concentration of ^{40}K in khat remained the highest in all the samples, followed by ^{226}Ra, and the least was ^{232}Th. The low levels of ^{232}Th and ^{226}Ra in khat can be attributed to the fact that these radionuclides are not involved in plant metabolic processes, preventing their accumulation (Saenboonruang et al., 2018). The relatively higher concentrations of ^{226}Ra in khat compared to ^{232}Th may be due to radium's chemical similarity to calcium, an essential mineral for plant growth (Chandrashekara & Somashekarappa, 2015). ^{226}Ra and calcium exhibit several chemical behaviours; both belong to Group 2 in the periodic table, react with water to form hydroxides and release hydrogen gas, both elements form soluble salts, and the hydroxides of both elements are alkaline (Saenboonruang et al., 2018). Radium's chemical similarity to calcium leads to higher activity concentrations in plants compared to ^{232}Th. The elevated ^{40}K level in the analysed khat samples is due to its crucial role in maintaining the plant and its status as the most abundant organic mineral element in all plant cells (Saenboonruang et al., 2018). Whereas the concentrations of the radioactive elements in soil follow the order ^{40}K > ^{232}Th > ^{226}Ra, the mean concentration of the radioelements follows the order ^{40}K > ^{226}Ra > ^{232}Th. This study finding is inconsistent with those reported in Kenya and Ethiopia whose findings revealed that the activity in khat follows ^{40}K > ^{232}Th > ^{226}Ra.

Table 4.2: Activity concentrations of ^{232}Th, ^{40}K, and ^{226}Ra in khat from the Dadamu sub-county.

	Activity concentration in khat ($Bq\ kg^{-1}$)		
Sample code	**^{226}Ra**	**^{232}Th**	**^{40}K**
C1	1.85 ± 0.94	3.45 ± 0.58	209.05 ±7.91
C2	3.23 ± 0.30	2.97 ± 0.64	58.89 ± 2.71
C3	2.22 ± 0.54	0.88 ± 0.30	117.33 ± 6.58
C4	2.53 ± 1.20	3.93 ± 1.03	177.08 ± 6.30
C5	2.40 ± 1.57	1.12 ± 0.35	185.24 ± 1.35
C6	15.80 ± 1.64	14.45 ± 1.48	717.17 ± 6.53
C7	12.78 ± 1.62	11.10 ± 1.84	647.06 ± 13.10
C8	10.38 ± 1.51	11.13 ± 1.65	479.62 ±12.44
C9	7.99 ± 0.41	1.62 ± 0.50	96.81 ± 5.46
C10	13.31 ± 0.10	4.42 ± 3.32	275.94 ± 35.58
C11	7.14 ± 0.39	6.51 ± 1.20	587.94 ±12.45
Ave	7.24 ±1.56	5.6 ± 1.39	322.92 ±72.22
Min	1.85 ± 0.94	1.12 ±0.35	58.89 ±2.71
Max	93.06 ±8.01	106.36 ±7.26	717.33 ± 6.53

4.2.3 Comparison of activity concentrations of ^{232}Th, ^{40}K, and ^{226}Ra in soil and khat

The mean activity levels of radioelements in soil and khat vary from location to location. This variation may be attributed to geological disparities and soil radiochemical composition in the khat-growing areas (Tettey-larbi et al., 2013). The mean activity levels of ^{226}Ra, ^{232}Th, and ^{40}K in the soil exceeded those in the khat (see Figure 4.1). The relatively lower activity concentrations of ^{226}Ra and ^{232}Th in khat compared to soil are because plants have selective mechanisms for absorbing only essential elements, or are easily mistaken for essential ones. ^{226}Ra

is absorbed due to its chemical resemblance to calcium, while ^{232}Th, being less chemically similar to vital nutrients, is least absorbed (Saenboonruang et al., 2018). Furthermore, the low uptake of ^{226}Ra and ^{232}Th by plants is due to their tendency to form insoluble compounds in soil. Their low solubility makes it difficult for plants to absorb them through their roots (Saenboonruang et al., 2018).

As observed from Figure 4.1, the average ^{40}K activity concentration in the soil exceeded that in the khat samples. The probable explanation for this observation is that plants regulate ^{40}K uptake in response to their physiological needs. The plants will only absorb what is necessary for their growth and functioning, leaving an excess of ^{40}K in the soil (Saenboonruang et al., 2018).

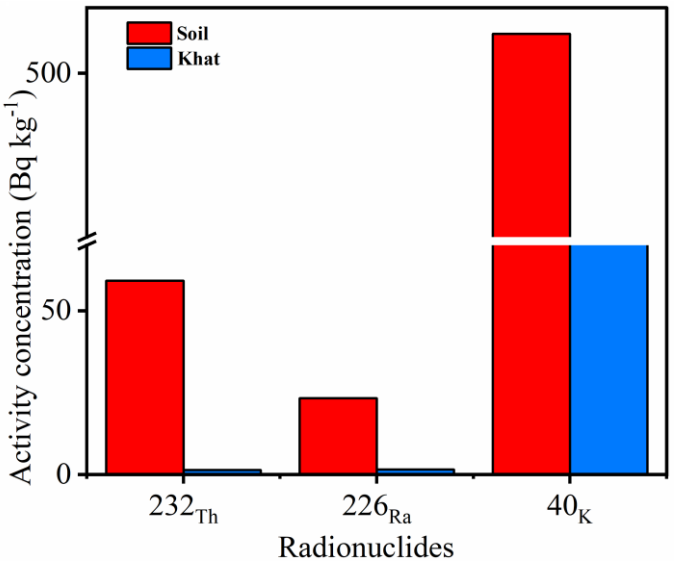


Figure 4.1: Average activity concentrations of ^{232}Th, ^{40}K, and ^{226}Ra in soil and khat.

Although the average ^{40}K activity concentration in soil was higher than in khat samples, in some sampling points, the ^{40}K activity concentration in khat exceeded that in the soil. The higher ^{40}K levels found in the analysed khat samples compared to the soil can be explained by the fact that this radionuclide plays a vital role in regulating plant metabolic activities such as photosynthesis, respiration, minerals

and nutrients uptake, and is the dominant mineral in every plant cell (Saenboonruang et al., 2018).

Comparisons of the average activities from this study's findings with those obtained elsewhere are summarised in Table A.1. The data extracted from Table A.1 are graphically presented as displayed in Figure 4.2. The average ^{40}K activity concentration in the soil (See Figure 4.2a) in the present study exceeded that in Nigeria (Kanayochukwu et al., 2022) and Kenya (Njagi et al., 2022) by 74% and 33%, respectively. However, the ^{40}K average soil activity level is lower than that of their counterparts in Bangladesh (Kabir et al., 2024) and Ethiopia (Techan, 2021) by 172% and 55%, respectively.

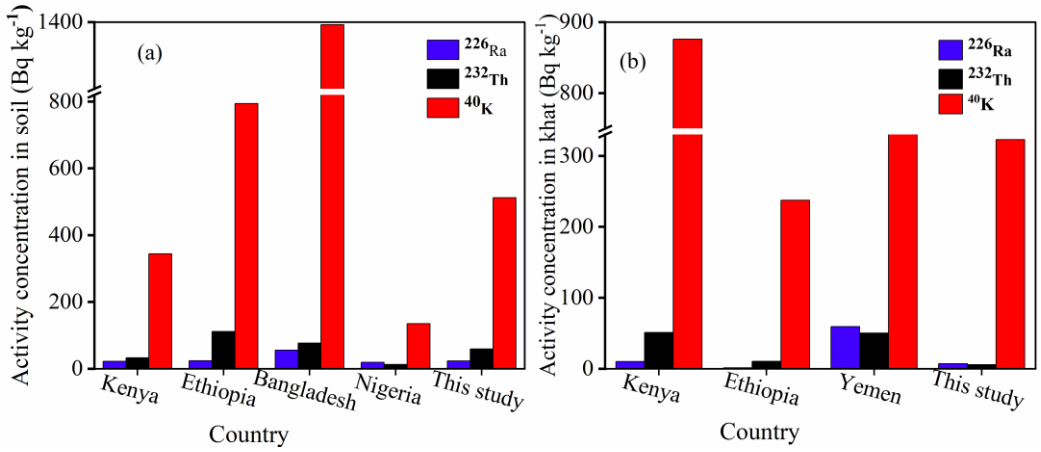


Figure 4.2: Average activity concentrations of ^{40}K, ^{232}Th, and ^{226}Ra in (a) soil and (b) khat from different countries.

The average ^{232}Th activity concentration in the soil in the present study exceeded those reported in Nigeria (Kanayochukwu et al., 2022) and Kenya (Ngari Vindensio Njagi, 2022) by 78% and 44%, respectively. In contrast, the mean ^{232}Th activity concentration was lower than those reported in Ethiopia and Bangladesh by 30% and 88%, respectively. Notably, the average ^{226}Ra activity concentration in the soil observed in this study is also similar to levels reported in Nigeria,

Ethiopia, and Kenya. However, the mean ^{226}Ra activity level is 138% below that reported in Bangladesh.

For khat (See Figure 4.2 b), the average ^{40}K activity level in this study is higher than that reported in khat from Ethiopia by 15%. In contrast, the average ^{40}K activity level in this study is just one-third of that reported in Kenya (Njagi et al., 2022) and about half of that reported in Yemen. The mean ^{232}Th activity level in this study is 85% lower than that reported for khat in Ethiopia. In addition, the average ^{232}Th activity concentration in this study is only one-tenth of that reported in Yemen and Kenya. The mean ^{226}Ra activity level recorded in this study is less than that reported in all the listed countries except for khat in Ethiopia.

4.3 Soil-to-plant transfer factors

The transfer factors (TF) were calculated using Equation (3.11) and are presented in Table A.2. The averages of soil-to-plant TF values for ^{40}K, ^{232}Th, and ^{226}Ra in the soil and khat were 0.97 ± 0.11, 0.11 ± 0.03, and 0.36 ± 0.09, respectively. A bar graph, based on data from Table A.2, comparing the average soil-to-plant TFs for ^{40}K, ^{232}Th, and ^{226}Ra in the Dadamu sub-county, is shown in Figure 4.3. It is observed from Figure 4.3 that the average TF of all the investigated radionuclides in the samples did not exceed 1 (Indicated by the red line). This indicates that, on average, the radionuclide concentration in soil exceeded that in khat. The high TFs for ^{40}K are attributed to its essential role in plants, where it performs various functions, including regulating enzyme activities, supporting photosynthesis, controlling plant growth, and enhancing metabolic processes (Mostafa & Farhan, 2021). The ability of ^{40}K to be more readily absorbed by plants from soil compared to other radionuclides is another contributing factor to its higher transfer factors. Additionally, ^{40}K plays a key role in boosting the immune system, increasing the

absorption of nitrogen and phosphorus, and facilitating the transport and accumulation of carbohydrates (Saenboonruang et al., 2018).

Furthermore, the average TFs for ^{232}Th and ^{226}Ra were less than that of ^{40}K. This observation implies that the average ^{232}Th and ^{226}Ra activity levels in the soil are far higher than those in khat samples, and therefore, khat does not accumulate these radionuclides. The extremely low mean TFs for ^{226}Ra and ^{232}Th could be because, in addition to these radionuclides not contributing significantly to plant metabolism, ^{226}Ra tends to bind more strongly to soil than to plants and is heavier than ^{40}K. Moreover, the TF values for ^{232}Th are the lowest, primarily because it is insoluble in water and immobile, as it strongly binds to organic matter and clay minerals (Vandenhove et al., 2009).

The TFs generally vary across all the sampling points. This may result from several factors, including soil organic matter content, particle size distribution, soil pH, soil type, levels of elements present, and the soil's capacity to absorb, retain, and transmit water (Mostafa & Farhan, 2021). The availability of nutrients for plant absorption depends on soil pH. For example, ^{40}K is generally available in the optimal pH range of 6.0 to 7.5, and as pH decreases (becomes more acidic), its availability diminishes. The optimal pH for the less soluble ^{232}Th is 4.0-5.0. Generally, its availability increases with increasing acidity (lower pH). ^{226}Ra is reported to be more soluble and mobile in acidic soils than in alkaline soils. The amount of soil organic matter significantly determines the soil-plant TF values for specific radionuclides, as it is the primary reservoir of certain nutrients. Through decomposition, the organic matter releases nutrients into the soil, making them available for absorption.

The calculated average TFs for the radionuclides were in the order: $^{40}K > ^{226}Ra > ^{232}Th$, which closely aligns with previously reported findings in Nigeria (Kanayochukwu et al., 2022). Compared with the reported mean ^{40}K TF value of 0.72 in Nigeria (Ugbede et al., 2021), the mean value observed in this study is 26% higher. In contrast, the mean TF of ^{40}K in the present study is lower than that reported in Vietnam (Thien et al., 2020) and approximately twice that reported in Iraq (Mostafa et al.

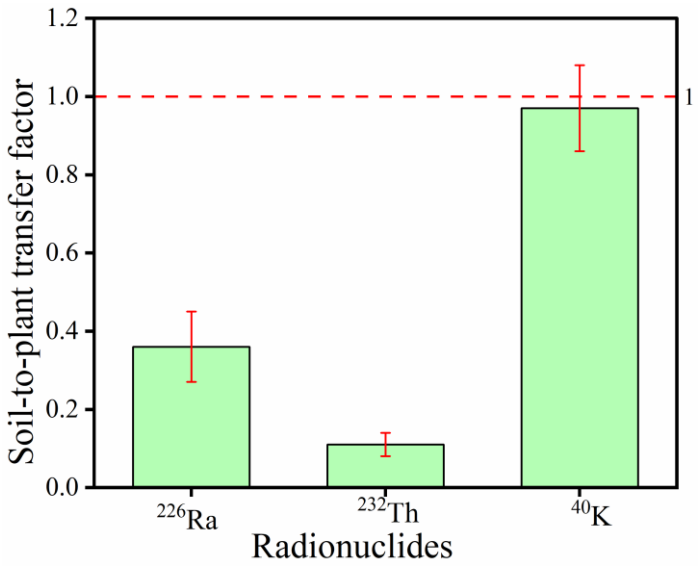


Figure 4.3: Average soil-to-plant transfer factor of ^{232}Th, ^{40}K, and ^{226}Ra from soil to khat from the Dadamu Sub-county.

4.4 Radiological hazard parameters in soil

The various radiological hazard parameters due to the investigated radionuclides in the soil were computed from the radionuclide's activity concentrations. The radiation hazards were evaluated using the radium equivalent activity (Ra_{eq}), absorbed dose rates (D_R), the annual effective dose equivalent due to outdoor exposure (E_{out}), and the ELCR. The results illustrated in Figure 4.4(a) are presented

in Table A.3. Additionally, the mean radiological values reported in other countries are shown in Table A.4 and presented graphically in Figure 4.4(b).

The Ra_{eq} refers to the total of the activity concentrations of ^{40}K, ^{232}Th, and ^{226}Ra calculated under the assumption that 130, 7, and 10 Bq kg^{-1} of ^{40}K, ^{232}Th, and ^{226}Ra, respectively, generate equal gamma dose rates (Sivakumar et al., 2015). The average Ra_{eq} in the investigated soil samples is 147.34 Bq kg^{-1}, and is 60% below the recommended world permissible limit of 370 Bq kg^{-1} (UNSCEAR, 2000). This indicates insignificant radiological hazards linked with the soil from the Dadamu sub-county. Comparison of the mean Ra_{eq} in this study with those reported in other countries (See Figure 4.4b) revealed that the mean Ra_{eq} value in this study is comparable with that reported in Indonesia (Murniasih & Prabasiwi, 2022). However, the observed mean Ra_{eq} in this study exceeded those reported in Nigeria (Ugbede et al., 2021), India (Sivakumar et al., 2015), Iraq (Alsaedi et al., 2020), and Korea (Lee et al., 2023) by 59%, 30%, 52%, and 40%, respectively.

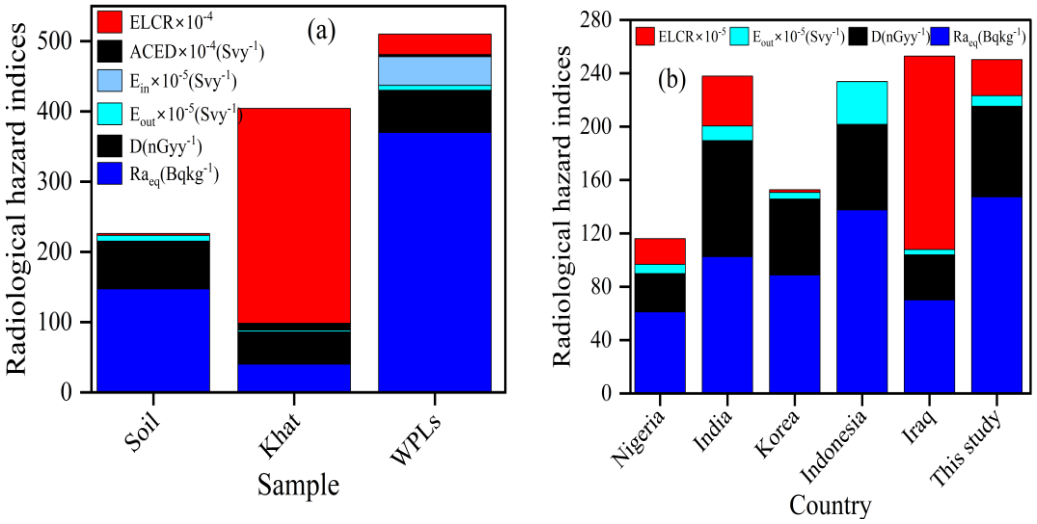


Figure 4.4: Radiological hazards in (a) Soil and Khat in this study and (b) Soils from other countries. The WPLs represent the world's permissible limits of radiological hazards.

The absorbed gamma dose rates (D_R) in outdoor air at 1 m were determined for each soil sample. The D_R values represented the amount of energy received from terrestrial ionising radiation per kilogram of matter per unit time. The calculated average of D_R in the soil is 67.86 nGy h^{-1}. This estimated mean gamma dose rate exceeded the global average of 59 nGy h^{-1} by 15% (Sivakumar et al., 2015). The D_R value alone does not indicate potential biological effects until it is transformed into the effective dose equivalent. The obtained average DR value is comparable to that reported in Indonesia (Murniasih & Prabasiwi, 2022) and is 28% lower than that reported in India (Sivakumar et al., 2015). In contrast, the mean absorbed rate due to soil in the present study exceeded the corresponding dose rates reported in Nigeria (Ugbede et al., 2021), Iraq (Alsaedi et al., 2020), and Korea (Lee et al., 2023) by 58%, 50%, and 16%, respectively.

To assess the impact of the absorbed gamma doses on the health of the inhabitants, the annual effective dose rates from outdoor exposure (E_{out}) were calculated. The average value of (E_{out}) is 0.0832 mSv y^{-1}. According to the UNSCEAR (Sivakumar et al., 2015), the world permissible limit of (E_{out}) is 0.46 mSv y^{-1}. Thus, the obtained average E_{out} is 82% below the world-permissible limit and poses no health threat to the inhabitants. Comparison of the average E_{out} value in the present with those reported in different countries around the world indicates that the observed average of E_{out} is comparable with those reported in Korea (Lee et al., 2023) and Nigeria (Ugbede et al., 2021), but greater than that reported in Iraq by 50%.

The likelihood of an individual developing cancer (ELCR) during his lifetime due to exposure to contaminated soil was computed from E_{out} values. The mean ELCR

obtained is 0.27×10^{-3}. The worldwide recommended maximum safe limit of ELCR is 0.29×10^{-3} (Abdelfadeel et al., 2023). Therefore, the calculated mean of ELCR is less than the world permissible limit by 6% and implies that the probability of developing cancer during one's lifetime from exposure to contaminated soil from the Dadamu Sub-county is very low. The observed average ELCR value in the present study is greater than those reported in Indonesia (Murniasih & Prabasiwi, 2022), Korea, and Nigeria (See Figure 4.4 b) by 99%, 93%, and 29%, respectively. However, the mean ELCR in the present study is lower than that reported in Iraq and India by 437% and 30%, respectively.

4.5 Radiological hazard parameters in khat

The radiological hazards considered due to khat ingestion were the Ra_{eq}, absorbed gamma dose rates (D_R), E_{out} and E_{in}, annual committed effective dose (ACED), and ELCR. The numerical values of the radiological hazard parameters are presented in Table A.5 and graphically in Figure 4.4, specifically in the central bar. In addition, the mean radiological hazard parameters for khat from other countries are presented in Table A.6 and presented graphically in Figure 4.5. The average Ra_{eq} is observed to be 40.11 Bq kg^{-1}, and this value is 89% lower than the world's permissible limit of 370 Bq kg^{-1}. This indicates that chewing khat produced from the Dadamu sub-county poses an insignificant health threat to humans. In addition, the estimated mean of Ra_{eq} exceeded those reported in Ethiopia (Techan, 2021) (See Figure 4.5) by 19%.

The average absorbed gamma dose rate was 20.19 nGy h^{-1}, 66% lower than the global average of 59 nGy h^{-1}. The low average D_R value, which falls below the threshold, is attributed to reduced activity concentrations of ^{40}K, ^{226}Ra, and ^{232}Th

in the khat, all of which were below their respective world-permissible limits. This implies that there is a lower risk of radiation-induced health issues that may result from chewing khat from the Dadamu sub-county.

The calculated values of E_{in} and E_{out} from exposure to contaminated khat are presented in Table A.5. The averages of E_{out} and E_{in} were 0.0248 and 0.0990 mSv y^{-1}, respectively. The UNSCEAR recommended 1 mSv y^{-1} to be the world's permissible limit for the E_{out} and E_{in} values. Therefore, the calculated averages of E_{out} and E_{in} were both below the world permissible limit. Furthermore, it is observed that the calculated averages of the annual equivalent doses were lower than the global averages of 0.07 and 0.41 mSv y^{-1} for E_{out} and (E_{in}), respectively (Abdelfadeel et al., 2023). This implies that the dose absorbed by an individual indoors or outdoors from radionuclides in khat grown in the Dadamu sub-county does not pose a significant health threat.

The ingestion dose from the intake of ^{40}K, ^{232}Th, and ^{226}Ra in khat (annual committed effective dose, $ACED_{ing}$) is a function of the quantity of radionuclides deposited on the khat and the daily consumption rate. The population-weighted mean of $ACED_{ing}$ in this study was 0.9703 mSv y^{-1} and exceeded the recommended world permissible limit of 0.87 mSv y^{-1} by 11% (UNSCEAR, 2000). This indicates that chewing khat from the Dadamu sub-county at the current rate (0.5 kg/day) can cause significant radiation-induced health risks to humans. In comparison, the population-weighted mean obtained in the current study is lower than that reported in Ethiopia by 139% and higher than that reported in Kenya by 54% (Njagi et al., 2022).

Although most radiological hazard values were below the globally accepted limits, the $ACED_{ing}$ of carcinogens from consuming khat exceeded the recommended safety threshold of 0.3 mSv y^{-1}. This indicates that the dose of radiation from ^{232}Th, ^{40}K, and ^{226}Ra in khat may present substantial cancer risks to the public with prolonged khat consumption. Therefore, it is essential to implement appropriate radiological safety measures, particularly regulating the consumption rates.

The average ELCR computed from the annual ingested dose of radiation was 3.06 $\times 10^{-3}$. This ECLR value is ten times the UNSCEAR recommended safe limit of 0.29×10^{-3} (UNSCEAR, 2000). This suggests a heightened risk of developing lung and kidney cancers arising from prolonged exposure to radiation as one consumes khat from the Dadamu sub-county at the chosen consumption rate.

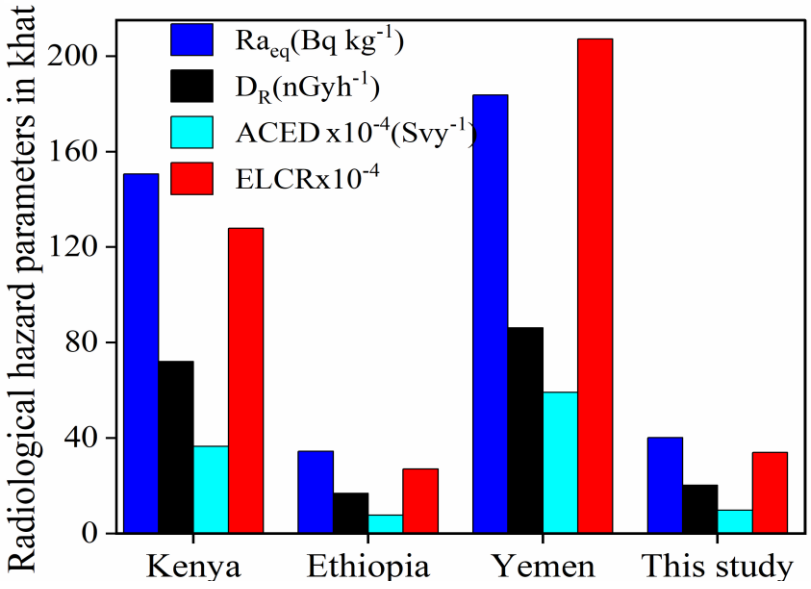


Figure 4.5: Radiological hazard parameters in khat from different countries.

4.6 Annual organ equivalent dose to different body parts

The yearly organ equivalent doses to 15 selected body organs from ingesting radionuclides in khat from the Dadamu sub-county were calculated using Rad Toolbox software. The results are recorded in Table 4.3. The computed annual

organ equivalent doses for all the body organs are presented in Table A.7. The mean annual organ equivalent doses were 0.8 μSvy^{-1} for ^{226}Ra, 2.22 $\mu Svy^{-1}$for ^{40}K, and 0.48 $\mu Svy^{-1}$for ^{232}Th. The colon, the upper large intestine, and the lower large intestine exhibited higher equivalent ^{40}K dose values than the other selected body organs. This is because, as food passes through the entire digestive tract, the intestinal muscles contract multiple times, helping to mix the food with the digestive enzymes to break it down (Kong & Singh, 2008). The tiny food fragments, decomposed by digestive organs, emit a certain level of radiation, which is transferred to adjacent organs when they come into contact with (Thien et al., 2020). Because the colon, lower large intestine, and upper large intestine are constantly in direct contact with the food being digested, they are expected to receive higher annual organ equivalent dose values (Reviews & Science, 2008).

The equivalent doses of ^{226}Ra and ^{232}Th to red marrow were 6.29 μSvy^{-1} and 2.63 μSvy^{-1}, respectively, higher than for all other organs. This is because both ^{226}Ra and ^{232}Th have a chemical affinity for calcium, leading to their deposition in bone tissue (Reviews & Science, 2008). Since red marrow is located within bones, these elements accumulate there (in the red marrow) over time. Another justification for the elevated annual equivalent doses of ^{226}Ra and ^{232}Th to red marrow is that these elements mimic calcium in the body's metabolic processes, causing them to be absorbed by bones, which house the red marrow (Thien et al., 2020).

Table 4.3: Yearly organ equivalent doses from ingestion of ^{232}Th, ^{40}K, and ^{226}Ra in Khat from Dadamu sub-county.

No.	Organ	Annual organ equivalent dose (μSv)			Total
		^{40}K	^{226}Ra	^{232}Th	
1	Breast	1.58	0.29	0.20	2.07
2	Brain	1.58	0.30	0.20	2.08
3	Stomach	1.81	0.30	0.20	2.31
4	Small Intestine	1.65	0.30	0.21	2.16
5	Kidneys	1.61	0.43	1.01	3.05
6	Upper large Intestine	3.13	0.46	0.28	3.87
7	Lower large Intestine	6.14	1.09	0.44	7.67
8	Ovaries	1.65	0.30	0.62	2.57
9	Red marrow	1.61	6.29	2.63	10.53
10	Colon	4.52	0.72	0.35	5.59
11	Lungs	1.61	0.29	0.20	2.10
12	Skin	1.55	0.29	0.20	2.04
13	Uterus	1.65	0.29	0.20	2.14
14	Spleen	1.61	0.38	0.20	2.19
15	extratracheal Airways	1.61	0.29	0.20	2.10
	Average	2.22	0.80	0.48	3.50

It is also observed that some organs have the same equivalent dose of a particular radionuclide. For example, the brain, stomach, and small intestine have 0.30

μSvy^{-1} of ^{226}Ra, while lungs, uterus, skin, spleen, breast, brain, stomach, and extratracheal airways have 0.2 μSvy^{-1} of ^{232}Th. This could probably be due to the uniform distribution. Radionuclides that are uniformly distributed throughout the body tend to be uniformly absorbed by multiple organs (Reviews & Science, 2008). This occurs most especially if the radionuclide circulates freely in the bloodstream and is not preferentially taken up by specific tissues. In addition, the proximity of some organs to the source of the radionuclide is another justification for the uniform absorption of that radionuclide. Organs located near each other may receive the same dose due to radiation from nearby tissues, particularly with penetrating radiation such as gamma rays (Reviews & Science, 2008).

The average yearly organ doses from radionuclides due to khat consumption are highest for ^{40}K, followed by ^{226}Ra, and then ^{232}Th. Organs retain large amounts of ^{40}K because it is a vital element involved in various biological functions, including regulating nerve activity, heart function, and muscle contractions (Thien et al., 2020).In comparison, the mean annual organ dose of the radionuclides in this work for ^{232}Th, ^{40}K, and ^{226}Ra was lower than that reported in Vietnam by 1275%, 1044%, and 750%, respectively (Thien et al., 2020).

4.7 Statistical Analysis

4.7.1 Pearson correlation analysis

Pearson's correlation coefficients were computed to quantify the strength of linear association between the activity concentrations of the radioelements and the corresponding radiological hazard indices. The results were presented in Figure 4.6. This analysis technique categorized correlation coefficients into five groups: negligible for ranges from (0.00-0.09), weak for the range (0.10-0.39), moderate

for the range (0.40-0.69), strong for the range (0.70-0.89), and very strong for the range (0.90-1.00). Figure 4.5 displays Pearson's correlation coefficients between the computed activity concentrations of ^{232}Th, ^{40}K, and ^{226}Ra and the estimated radiological hazard parameters in soil and khat. A strong positive correlation was observed between the ^{226}Ra and ^{232}Th activity concentrations, with coefficients of 0.79 for both soil and khat. This is because the decay series of ^{232}Th and ^{238}U, of which ^{226}Ra is one of the progenies, coexist in nature (Sivakumar et al., 2015). Similarly, a very strong correlation exists between the ^{232}Th and ^{40}K activity concentrations, with coefficients of 0.83 for soil and 0.91 for khat. This suggests that these radionuclides are associated with similar geological or environmental factors, such as common source rocks (Taylor et al., 2014).

(a) Soil (b) Khat

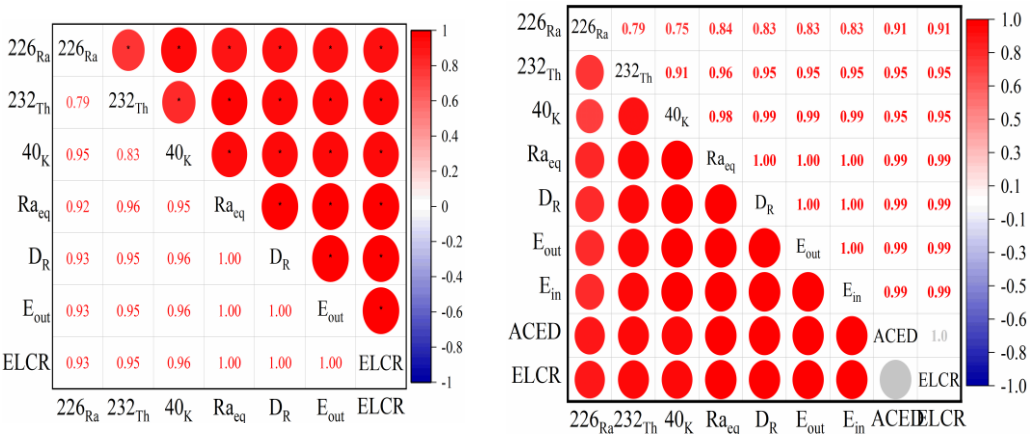


Figure 4.6: Heat map illustrating Pearson's correlation analysis of activity concentration of radionuclides and the radiological hazard indices in (a) soil and (b) khat.

It should also be noted that very high correlations (with $r \geq 0.95$ in both soil and khat) exist between the activity concentrations of ^{232}Th and ^{40}K, along with all radiological hazard parameters. Since ^{40}K is an essential element for plants and is

relatively abundant in soil, its activity concentration does not control the level of radiological hazards. This suggests that the magnitude of the radiological hazard parameters in soil and khat is primarily controlled by ^{232}Th levels (Sivakumar et al., 2015).

The colour blue denotes a negative correlation, while red denotes a positive correlation. Pearson's correlation coefficients are indicated in (a) the lower triangle and (b) the upper triangle.

Another significant finding is the existence of a very high positive correlation among the radiological hazard parameters. This is because these hazard parameters depend directly on the radioelement's activity levels. Specifically, most radiological hazard parameters are derived using similar mathematical expressions based on the activity levels of these radionuclides.

4.7.2 Principal component analysis

Principal component analysis (PCA) was performed to identify which radionuclides contribute most to the overall radiological risk in the Dadamu sub-county. The same variables were used for the PCA and the Pearson correlation analysis. Table A.8(a) presents the principal components obtained, labelled as principal component one (PC1) and principal component two (PC2), along with the corresponding proportions of the variances explained. Factor loadings define the correlations between the variables and the derived principal components. It indicates how much a particular principal component explains a given variable.

For soil, the coefficients of the principal components are presented in Table A.8(a) and graphically in Figure 4.7(a). The PC1 derived from weak loadings of ^{232}Th and the associated radiological hazard parameters has an explained variance of

95.55%. However, the PC2 extracted from moderate loading of ^{226}Ra and ^{40}K showed negligible negative correlations with the associated hazard parameters, with an explained variance of 3.71%. This demonstrates that the overall level of radioactivity arising from the soil in Dadamu Sub-county is due to ^{232}Th activity concentration.

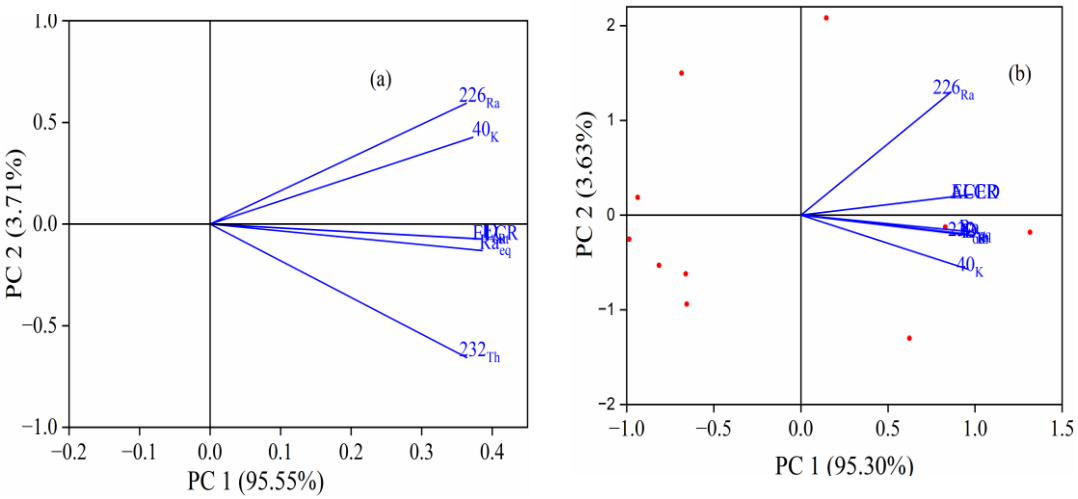


Figure 4.7: Graphical representations of the PCA between the activity concentrations of ^{40}K, ^{226}Ra, and ^{232}Th and the radiological hazard parameters in (a) soil and (b) khat from Dadamu Sub-county.

For khat, its corresponding principal component coefficients are recorded in Table A.8(b) and graphically illustrated in Figure 4.7(b). It is worth noting that the principal PC1, with an explained variance of 95.30%, is weakly positively loaded with ^{232}Th and ^{40}K, as well as the radiological hazard parameters. Conversely, the principal component 2, which accounts for only 3.63% of the total variance, has a negative loading on ^{40}K. In this study, the two principal components explain 98.93% of the radioactive variance. According to the recommendation by Ravikumar et al (Ravikumar & Somashekar, 2014), an ordination result is considered good if more than 75% of the variance is explained. From PC1, we can conclude that ^{232}Th is the main contributing radionuclide to the radiological

hazards from khat ingestion in the Dadamu Sub-County. The PCA analysis of soil and khat in the studied area revealed that ^{232}Th activity concentrations primarily influence the radiological hazard levels in the Dadamu sub-county, aligning with Pearson's correlation analysis.

4.7.3 Hierarchical cluster analysis

The software OriginPro 2024 was used to conduct Hierarchical cluster analysis (HCA) to determine how activity concentrations affect radiological hazard levels in both soil and khat. HCA is a data classification technique that uses a multivariate approach to group variables into clusters based on their similarities. It involves categorising variables with similar traits into one cluster. The process starts by grouping the variables with the highest level of similarity, and continues until all the data sets are organised into clusters based on their similarities. A dendrogram displays the trend in which variables merge to produce clusters with identical characteristics. The level of similarity between variables decreases as the height of merging increases; completely identical variables (100% similar) merge at negligible heights, whereas those that are more dissimilar (0% similar) merge at the greatest height (Sivakumar et al., 2015). The derived dendrograms for the HCA of soil and khat are displayed in Figure 4.8 (a) and (b), respectively.

Figure 4.8 (a) illustrates a strong similarity between ^{232}Th and the entire set of radiological hazard parameters, as they are grouped in the same cluster (Cluster 1). This indicates that the radiological hazard levels in the soil of the Dadamu sub-county depend entirely on the ^{232}Th activity concentration. Cluster II consists of ^{226}Ra and ^{40}K, with no similarity to radiological hazard indices, indicating that the activity concentrations of ^{226}Ra and ^{40}K do not significantly contribute to the radiological hazards associated with soil.

In khat (see Figure 4.8b), ^{40}K activity levels are grouped into a single cluster containing all radiological hazards, with weak similarity (Cluster 1). However, ^{40}K, being an essential, does not determine the radiological hazards in the plant. Cluster II consisted of ^{226}Ra and ^{232}Th, but ^{232}Th showed greater similarity (about 70%) to radiological hazards than 226Ra (about 0%). This observation indicates that the radiological hazard levels in khat are primarily determined by the activity concentrations of ^{232}Th. In contrast, ^{226}Ra contributes the least to radiological hazards in khat, consistent with the PCA findings.

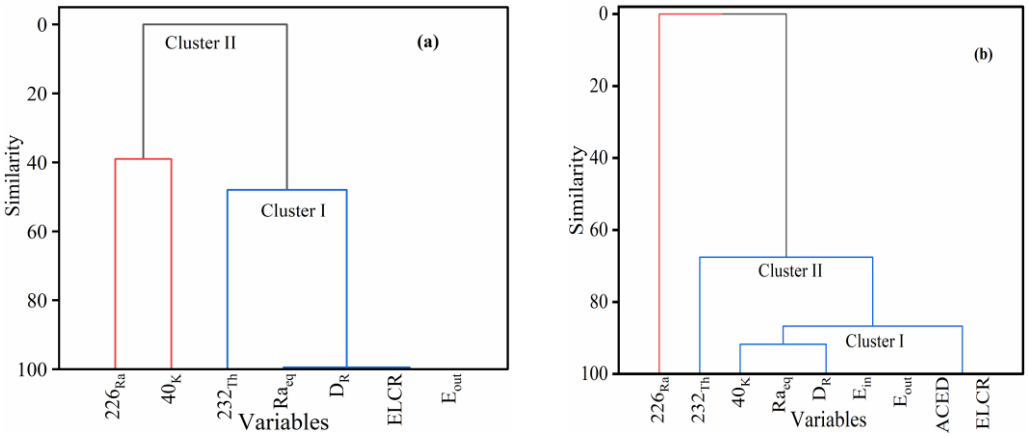


Figure 4.8: Dendrograms for the HCA of (a) Soil and (b) Khat from the Dadamu sub-county.

CHAPTER FIVE: CONCLUSION AND RECOMMENDATIONS

5.1 Conclusion

The activity levels of the radionuclides in the eleven pairs of soil and khat samples from the Dadamu-Sub-county were analysed using an HPGe detector. The mean activity concentrations of ^{232}Th, ^{40}K, and ^{226}Ra in soil were 59.16 ± 13.55, 512.05 ± 149.27, and 23.32 ± 5.59 Bq kg^{-1}, respectively. The mean activity concentrations of ^{232}Th, ^{40}K, and ^{226}Ra in khat were 5.60 ± 1.39, 322.92 ± 72.22, and 7.24 ± 1.56 Bq kg^{-1}. The mean activities of ^{232}Th, ^{40}K, and ^{226}Ra in khat did not exceed the internationally accepted thresholds. In soil samples, ^{232}Th and ^{40}K activities exceeded the recommended safe limits, while ^{226}Ra activity concentration was below the world permissible limit. This suggests that the soil in the Dadamu sub-county is suitable for cultivation.

For soil, average radiological hazard parameters were 147.34 Bq kg^{-1} for Ra_{eq}, 67.68 nGy h^{-1} for the absorbed dose rates, 0.08 μSvy^{-1} for the E_{out}, and 0.27× 10^{-3} for the ELCR. The mean of all the radiological hazards in soil was within the world's permissible limits, except for absorbed dose rates. For khat, however, the average radiological hazard parameters were 40.11 Bq kg^{-1} for Ra_{eq}, 20.19 nGy h^{-1} for the absorbed dose rates, 0.0248 μSvy^{-1} for E_{out}, 0.099 μSvy^{-1} for E_{in}, 0.9703 μSv$y^{-1}$for annual committed effective dose, and 3.06× 10^{-3} for the ELCR. The averages of the Ra_{eq}, D_R, the E_{out}, and the E_{in} were below the world's permissible limits. Nevertheless, the average ACED and excess ELCR were slightly above the safety thresholds as recommended by USEPA. This indicates that prolonged chewing of khat produced from the Dadamu sub-county may lead to significant health issues if the consumption levels are not controlled.

Statistical analysis using Pearson correlation revealed a very high positive correlation between the activity concentrations of ^{232}Th, ^{40}K, and ^{226}Ra and the radiological hazard indices. Further statistical analysis using PCA and HCA revealed that ^{232}Th significantly contributes to the radiological hazards in both soil and khat. In contrast, ^{226}Ra contributes the least to the radiological hazards in khat from the Dadamu sub-county.

5.2 Recommendations

1. This study did not account for variation in radionuclide activity concentrations with counting time, in addition to the small sample size. Longer counting time increases the number of detected counts in each photopeak. Only 6 hours of counting time could have negatively affected the determined activity concentrations and the corresponding hazards. Future studies should use more extended measurement periods and larger sample sizes to achieve better results.
2. The study used standard conversion factors such as the dose coefficients and occupancy factors from UNSCEAR and ICRP. It also adopted a foreign khat consumption rate of 0.5 kg per day for computing the radiological hazard parameters. These assumptions may not accurately represent the actual habits and conditions of the inhabitants. Future researchers should consider the use of localised dose coefficients and khat consumption rates to enhance accurate results.
3. This research did not account for the variations in the radionuclide's activity concentrations between wet and dry seasons due to leaching and deposition. This could have influenced radionuclide distribution, as only the dry season was considered. Future studies should incorporate seasonal sampling for meaningful results.

REFERENCES

Abdelfadeel, E. H., El-Halim, E. S. A., Hegazy, T. M., & Ghany, H. A. A. (2023). *Relationship between radioactivity and toxicity in some medicinal plants. Scientific Reports*, *13*(1). https://doi.org/10.1038/s41598-023-37403-7

Abojassim, A. A., Al-gazaly, H. H., & Kadhim, S. H. (2014). *Estimated the radiation hazard indices and ingestion effective dose in wheat flour samples of Iraq markets*. 1–5.

Ajayi, O. S., Dike, C. G., & Balogun, K. O. (2018). Elemental and radioactivity analysis of rocks and soils of some selected sites in southwestern Nigeria. *Environmental Forensics*, *19*(2), 87–98. https://doi.org/10.1080/1527 5922 .2018.1448906

Al-jalali, M. A., & Shaltout, A. A. (2014). *Natural Radioactivity of Catha edulis (Khat) and Tobacco plants collected from Yemen*. *(IJIRSE) International Journal of Innovative Research in Science & Engineering*, *2*(5), 350–354.

Alsaedi, J. K., Hasan, N. M., & Abdulhasan, A. A. (2020). *Natural radioactivity in soil samples from selected area in Nineveh Governorate, Iraq*. *21*, 187–194.

Aparecida, J., García-tenorio, R., & Marcos, D. (2017). *Natural radionuclides in plants , soils and sediments affected by U-rich coal mining activities in Brazil*. *177*, 37–47. https://doi.org/10.1016/j.jenvrad.2017.06.001

Asfaw, L. S. (2023). *Adverse Effects of Chewing Khat (*. *38*(1), 8–10. https://doi.org/10.5001/omj.2023.46

Azhdarpoor, A., Hoseini, M., Shahsavani, S., & Shamsedini, N. (2021). *Assessment of excess lifetime cancer risk and risk of lung cancer due to exposure to radon in a middle eastern city in Iran*. *Radiation Medicine and Protection*, *2*(3), 112–116. https://doi.org/10.1016/j.radmp.2021.07.002

Biira, S., Ochom, P., & Oryema, B. (2021). *Evaluation of radionuclide concentrations and average annual committed effective dose due to medicinal plants and soils commonly consumed by pregnant women in Osukuru , Tororo (Uganda). Journal of Environmental Radioactivity,* 227(June 2020), 106460. https://doi.org/10.1016/j.jenvrad.2020.106460

Buchtela, K. (2019). Radiochemical methods | Gamma-Ray Spectrometry q. In *Encyclopedia of Analytical Science* (Third Edit, Vol. 9, Issue August 2014). Elsevier. https://doi.org/10.1016/B978-0-12-409547-2.11333-2

Chandrashekara, K., & Somashekarappa, H. M. (2015). ScienceDirect *Estimation of radionuclides concentration and average annual committed effective dose due to ingestion for some selected medicinal plants of*. *Journal of Radiation Research and Applied Sciences*, *9*(1), 68–77. https://doi.org/ 10.1016/ j.jrras. 2015.09.005

Hafızoğlu, N. (2024). *Efficiency and energy resolution of gamma spectrometry system with HPGe detector depending on variable source-to-detector distances. European Physical Journal Plus*, *139*(2), 1–9. https://doi.org/10.1140/epjp/s13360-024-04903-y

International Atomic Energy Agency. (2019). Guidelines on soil and vegetation sampling for radiological monitoring. *Technical Reports Series No. 486*, *486*.

International, I. E. A., & Agency, E. (2023). *Uganda 2023 Energy Policy Review*.

Kabir, S., Amirul, M., & Belal, M. (2024). *Journal of Radiation Research and Applied Sciences Natural radioactivity in soils and medicinal plants of the Sundarban : Concomitant radiological risks and radionuclide transfer factor. Journal of Radiation Research and Applied Sciences*, *17*(4), 101071. https://doi.org/10.1016/j.jrras.2024.101071

Kanayochukwu, J., Chisom, T., Ijeoma, H., Chijioke, P., & Chioma, P. (2022). *Case Studies in Chemical and Environmental Engineering Health risk assessment of radiation dose of background radionuclides in quarry soil and uptake by plants in Ezillo-Ishiagu in Ebonyi*. *Case Studies in Chemical and Environmental Engineering*, *6*(October), 100269. https://doi.org/ 10.1016/j.cscee.2022.100269

Kolapo, A. A., & Oluwatosin, J. (2018). *Health Risk Assessment of Natural Radionuclide and Heavy Metals in Commonly Consumed Medicinal Plants in South-west*. *20*(3), 529–537.

Kong, F., & Singh, R. P. (2008). *Disintegration of solid foods in human stomach*. *Journal of Food Science*, *73*(5), 67–80. https://doi.org/10.1111/j.1750-3841.2008.00766.x

Lee, J., Kim, H., Uk, Y., Yeon, D., Soon, W., Geun, C., Kee, J., Baek, J., & Kang, Y. (2023). *Activity concentrations and radiological hazard assessments of 226 Ra , Th , 40 K , and 137 Cs in soil samples obtained from the Dongnam Institute of Radiological & Medical Science , Korea. Nuclear Engineering and Technology*, *55*(7), 2388–2394. https://doi.org/10.1016/j.net.2023.03.022

Little, M. P., Wakeford, R., Zablotska, L. B., Borrego, D., Grif, K. T., Allodji, R. S., Vathaire, F. De, Lee, C., Brenner, A. V, Miller, J. S., Campbell, D., Pearce, M. S., Sadetzki, S., Doody, M. M., Holmberg, E., Lundell, M., French, B., & Adams, M. J. (2023). *Radiation exposure and leukaemia risk among cohorts of persons exposed to low and moderate doses of external ionising radiation in childhood*. *December 2022*. https://doi.org/10.1038/ s41416-023-02387-8

Luis, J., & Orcid, J. (2024). Radioactive isotopes theft in Mexico during 2011–2023: a green criminological approach. *Crime Prevention and Community*

Safety, 347–369. https://doi.org/10.1057/s41300-024-00215-6

Manchikanti, L., Pasupuleti, R., Pampati, V., Sanapati, M. R., & Hirsch, J. A. (2023). *Assessment of radiation exposure with mandatory two fluoroscopic views for epidural procedures. Pain Physician*, *26*(7), 557–567.

McColl, N., Auvinen, A., Kesminiene, A., Espina, C., Erdmann, F., de Vries, E., Greinert, R., Harrison, J., & Schüz, J. (2015). European Code against Cancer 4th Edition: Ionising and non-ionising radiation and cancer. *Cancer Epidemiology*, *39*, S93–S100. https://doi.org/10.1016/j.canep.2015.03.016

Mostafa, M. Y. A., & Farhan, N. (2021). The plant transfer factor of natural radionuclides and the soil radiation hazard of some crops. *Environmental Monitoring and Assessment*. https://doi.org/10.1007/s10661-021-09061-7

Muller, S., Ader, I., Justine, C., Leménager, H., Achard, P., Casteilla, L., Sensebé, L., Carrière, A., & Deschaseaux, F. (2019). *Human adipose stromal-vascular fraction self-organizes to form vascularized adipose tissue in 3D cultures*. *December 2018*, 1–10. https://doi.org/10.1038/s41598-019-43624-6

Murniasih, S., & Prabasiwi, D. S. (2022). *Assessment of Radiological Hazards in Soil , Water and Plants Around Coal Power Plant*. *V*(xxx), 137–145.

Ngari Vindensio Njagi. (2022). *Levels of Natural Raionuclides in Khat (Catha Eduils) Leaves and soil in Selected Areas in Embu County, Kenya*.

Njagi, N. V., Hashim, N., & Abdallah, M. (2022). *Levels Of Natural Radionuclides in Khat (Catha Edulis) Leaves and Soils In Selected Areas In Embu County , Kenya*. *2*(3), 566–579.

Nyakecho, C., & Hagemann, S. G. (2024). Australian Journal of Earth Sciences : *An International Geoscience Journal of the Geological Society of Australia An overview of gold systems in Uganda*. *Australian Journal of Earth Sciences*,

60(8), 1–30. https://doi.org/10.1080/08120099.2013.831773

Odumo, O. B., Mustapha, A. O., Patel, J. P., & Angeyo, H. K. (2011). *Radiological survey and assessment of associated activity concentration of the naturally occurring radioactive materials (NORM) in the Migori artisanal gold mining belt of southern Nyanza, Kenya*. *Applied Radiation and Isotopes*, *69*(6), 912–916. https://doi.org/10.1016/j.apradiso.2011.02.016

Olagbaju, P. O., Wojuola, O. B., & Tshivhase, V. (2021). Radionuclides Contamination in Soil: Effects, Sources and Spatial Distribution. *EPJ Web of Conferences*, *253*, 09006. https://doi.org/10.1051/epjconf/202125309006

Paleari, C. I., Mekhaldi, F., Adolphi, F., Christl, M., Vockenhuber, C., Gautschi, P., Beer, J., Brehm, N., Erhardt, T., Synal, H. A., Wacker, L., Wilhelms, F., & Muscheler, R. (2022). *Cosmogenic radionuclides reveal an extreme solar particle storm near a solar minimum 9125 years BP*. *Nature Communications*, *13*(1). https://doi.org/10.1038/s41467-021-27891-4

Pervin, S., Yeasmin, S., Khandaker, M. U., & Begum, A. (2022). Radon Concentrations in Indoor and Outdoor Environments of Atomic Energy Centre Dhaka, Bangladesh, and Concomitant Health Hazards. *Frontiers in Nuclear Engineering*, *1*(June), 1–10. https://doi.org/10.3389/ fnuen.2022.901818

Ravikumar, P., & Somashekar, R. K. (2014). *Determination of the radiation dose due to radon ingestion and inhalation. International Journal of Environmental Science and Technology*, *11*(2), 493–508. https://doi.org/10.1007/ s13762-013-0252-x

Reguigui, N. (2014). Gamma Ray Spectrometry Practical Information. *Reguigui, N. (2014*, *January*, 4–79.

Reviews, C., & Science, F. (2008). *Disintegration of Solid Foods in Human Stomach*. *73*(5), 67–80. https://doi.org/10.1111/j.1750-3841.2008.00766.x

Saenboonruang, K., Phonchanthuek, E., & Prasandee, K. (2018). *Determination Using Gamma Spectroscopy of Natural Radionuclide Activity Concentrations and Annual Committed Effective Doses in Selected Thai Medicinal Plants*. *45*(2), 821–831.

Sharon, B. A., Nakaganda, A., Fadhil, G., June, M., Anecho, E., Aniku, G., Jacinto, A., Wao, H., Orem, J., & Daniel, O. (2024). *Cancer patterns in Arua district , Uganda : a hospital-based retrospective study*. 1–15.

Silva, B., Soares, J., & Rocha-pereira, C. (2022). *Khat , a Cultural Chewing Drug : A Toxicokinetic and Toxicodynamic Summary*. 1–12.

Singh, A. K., & Bhargawa, A. (2020). *Delineation of possible influence of solar variability and galactic cosmic rays on terrestrial climate parameters. Advances in Space Research*, *65*(7), 1831–1842.https:// doi.org/10.1016/ j.asr.2020.01.006

Sivakumar, S., Chandrasekaran, A., Ravisankar, R., Ravikumar, S. M., Prince Prakash Jebakumar, J., Vijayagopal, P., Vijayalakshmi, I., & Jose, M. T. (2015). *Measurement of natural radioactivity and evaluation of radiation hazards in coastal sediments of east coast of Tamilnadu using statistical approach. Journal of Taibah University for Science*, *8*(4), 375–384. https://doi.org/10.1016/j.jtusci.2014.03.004

Storer, E., Anguyo, I., Odda, A., & Storer, E. (2022). *“ One Man ’s Meat Is Another Man ’s Poison ’: Marungi and Realities of Resilience in North West Uganda “ One Man ’s Meat Is Another Man ’s Poison ’: Marungi and Realities of Resilience in North West Uganda. Civil Wars*, *00*(00), 1–26.

https://doi.org/10.1080/13698249.2022.2031440

Taylor, P., Nyakecho, C., & Hagemann, S. G. (2014). *Australian Journal of Earth Sciences : An International Geoscience Journal of the Geological Society of Australia An overview of gold systems in Uganda An overview of gold systems in Uganda*. *June*, 37–41. https://doi.org/ 10.1080/ 08120099.2013.831773

Techan, M. (2021). *Assessment and Investigation of Natural Radioactivity Levels in Leaves of Khat and Agricultural Soil Samples Collected from Haramaya , East Hararghe , Ethiopia , Using Gamma Spectrometry A thesis Submitted to the Department of Physics , Addis Ababa Univer*.

Teni, F., Surur, A., Hailemariam, A., Aye, A., Mitiku, G., Gurmu, A., & Tessema, B. (2015). *Prevalence, reasons, and perceived effects of Khat chewing among students of a college in Gondar town, Northwestern Ethiopia: A cross-sectional study*. *Annals of Medical and Health Sciences Research*, *5*(6), 454. https://doi.org/10.4103/2141-9248.177992

Tesfaye, E., Krahl, W., & Alemayehu, S. (2020). Khat induced psychotic disorder: Case report. *Substance Abuse: Treatment, Prevention, and Policy*, *15*(1), 1–5. https://doi.org/10.1186/s13011-020-00268-4

Tettey-larbi, L., Darko, E. O., Schandorf, C., & Appiah, A. A. (2013). *Natural radioactivity levels of some medicinal plants commonly used in Ghana*. 1–9.

Thien, B. N., Ba, V. N., Vy, N. T. T., & Loan, T. T. H. (2020). Estimation of the soil to plant transfer factor and the annual organ equivalent dose due to ingestion of food crops in Ho Chi Minh city, Vietnam. *Chemosphere*, *259*, 127432. https://doi.org/10.1016/j.chemosphere.2020.127432

Truc, H., Ngoc, V., Ngoc, B., Truong, L., & Hong, T. (2023). Accumulation and distribution of nutrients , radionuclides and metals by roots , stems and leaves

of plants. *Nuclear Engineering and Technology*, *55*(7), 2650–2655. https://doi.org/10.1016/j.net.2023.03.039

Turyahabwa, E. R. S. (2024). *Assessing the radiological hazards due to radionuclides in sediments and tailings around Kilembe copper mines , Western Uganda*. 1–18.

Tyovenda, A. A., Ocheje, J. A., Terver, S., & Uttah, E. U. (2022). *Investigation of the Radiological Risk of Farmlands and the Transfer Factor from Soil to Crops in Jalingo and Wukari L.G.A of Taraba State, Nigeria*. *Journal of Environmental Protection*, *13*(01), 1–14. https://doi.org/ 10.4236/ jep.2022.131001

UBOS. (2024). U*ganda Bureau of Statistics theme: Building a Country We All Cherish Securing The Future Through Statistics*.

Uganda Investment Authority. (2021). A*rua District Investment Profile: Uganda Investment Authority*. https://www.westnileweb.com

Ugbede, F. O., Osahon, O. D., & Agbalagba, E. O. (2021). *Radiological Risk Assessment of ^{238}U, ^{232}Th and ^{40}K in Soil and Their Uptake by Rice Cultivated in CAS Paddy Environment of Abakaliki, Nigeria. Chemistry Africa*, *4*(3), 691–701. https://doi.org/10.1007/s42250-021-00244-w

Ullah, F., Muhammad, S., & Ali, W. (2022). *Radon concentration and potential risks assessment through hot springs water consumption in the Gilgit and Chitral, Northern Pakistan. Chemosphere*, *287*(P3), 132323. https://doi.org/10.1016/ j.chemosphere.2021.132323

UNSCEAR. (2000). S*ources and Effects United Nations Scientific Committee on the Effects of Atomic Radiation: Vol. I*.

Vandenhove, H., Olyslaegers, G., Sanzharova, N., Shubina, O., Reed, E., Shang,

Z., & Velasco, H. (2009). *Proposal for new best estimates of the soil-to-plant transfer factor of U , Th , Ra , Pb and Po. Journal of Environmental Radioactivity*, *100*(9), 721–732. https://doi.org/ 10.1016/ j.jenvrad.2008.10.014

Wabe, N. T. (2011). Chemistry, pharmacology, and toxicology of khat (catha edulis forsk): a review. *Addiction & Health*, *3*(3–4), 137–149. http://www.ncbi.nlm.nih.gov/pubmed/24494129%0Ahttp://www.pubmedcentral.nih.gov/articlerender.fcgi?artid=PMC3905534

Zhakypbek, Y., Toktar, M., Kossalbayev, B. D., Baktygali, A., & Kamarkhan, Z. (2025). *Effects of Gold Mining on the Physicochemical Properties of Soils at the Akbakai Gold Deposit*. 1–15.

Zhang, L., Chu, J., Xia, B., Xiong, Z., Zhang, S., & Tang, W. (2022). *Health Effects of Particulate Uranium Exposure*. *Toxics*, *10*(10). https://doi.org/10.3390/ toxics10100575

APPENDICES

Appendix A

Table A.1: Avera

ge activity concentrations of ^{232}Th, ^{40}K, and ^{226}Ra in soil and khat from different countries.

Country	Samples	Activity concentrations (Bq/kg)			Reference
		^{226}Ra	^{232}Th	^{40}K	
Kenya	soil	22.00	33.00	344.00	(Njagi et al., 2022)
	khat	10.10	51.10	875.80	
Uganda	soil	23.32	59.16	512.05	This study
	khat	7.24	5.60	322.92	
Ethiopia	Soil	23.72	111.50	794.10	(Techan, 2021)
	Khat	1.32	10.36	273.39	
Bangladesh	soil	55.60	76.70	1392.50	(Kabir et al., 2024)
Nigeria	soil	19.09	12.78	134.77	(Kanayochukwu et al., 2022)
Yemen	khat	59.50	50.30	678.00	(Al-jalali & Shaltout, 2014)

Table A.2: The soil-to-plant transfer factors of ^{232}Th, ^{40}K, and ^{226}Ra for soil and khat samples from the Dadamu cub county**.**

Sample codes	Soil-to-plant transfer factor		
	^{226}Ra	**^{232}Th**	**^{40}K**
C1	0.08 ± 0.04	0.03 ± 0.01	0.34 ± 0.02
C2	0.20 ± 0.03	0.03 ± 0.01	0.10 ± 0.01
C3	0.12 ± 0.03	0.03 ± 0.01	0.57 ± 0.05
C4	0.19 ± 0.09	0.16 ± 0.04	2.48 ± 0.64
C5	0.67 ± 0.44	0.13 ± 0.04	1.74 ± 0.10
C6	0.21 ± 0.02	0.09 ± 0.01	0.38 ± 0.01
C7	0.54 ± 0.07	0.28 ± 0.06	1.00 ± 0.02
C8	0.46 ± 0.08	0.20 ± 0.03	0.96 ± 0.05
C9	0.60 ± 0.09	0.12 ± 0.07	0.25 ± 0.02
C10	0.59 ± 0.09	0.07 ± 0.05	0.75 ± 0.10
C11	0.30 ± 0.01	0.12 ± 0.02	2.08 ± 0.18
Ave	0.36 ± 0.09	0.11 ± 0.03	0.97 ± 0.11

Table A.3: The radiological hazard parameters in soil samples from the Dadamu Sub-county.

Sample codes	$\mathbf{Ra_{eq}}$ $(\mathbf{Bq\ kg^{-1}})$	**Dose** $(\mathbf{nGy\ h^{-1}})$	$\mathbf{E_{out}}$ $(\mathbf{mSv\ y^{-1}})$	**ELCR**$\times$ $\mathbf{10^{-3}}$
C1	227.56	102.62	0.1259	0.4027
C2	202.03	91.15	0.1118	0.3577
C3	73.43	33.62	0.0412	0.1319
C4	55.08	24.45	0.0300	0.0959
C5	24.42	11.43	0.0140	0.0449
C6	439.59	205.96	0.2526	0.8083
C7	130.04	61.82	0.0758	0.2426
C8	141.82	65.40	0.0802	0.2566
C9	63.06	30.77	0.0377	0.1208
C10	141.35	63.97	0.0785	0.2511
C11	122.35	55.22	0.0677	0.2167
Ave	147.34	67.86	0.0832	0.2663

Table A.4: Comparison of the radiological hazard parameters in soil in this study with other studies around the world.

Country	Ra_{eq} ($Bq\ kg^{-1}$)	D($nGyh^{-1}$)	E_{out} ($mSvy^{-1}$)	ELCR($\times 10^{-3}$)
Nigeria	61.12	28.66	0.07	0.192
India	102.56	86.95	0.11	0.374
Indonesia	137.51	64.14	0.32	0.001
Korea	88.77	56.92	0.05	0.020
Iraq	70.04	33.83	0.04	1.450
Uganda	147.34	67.86	0.08	0.270

Table A.5: Radiological hazard parameters due to ingestion of khat from the Dadamu Sub-county.

Sample Codes	Ra_{eq} (Bq kg^{-1})	D ($nGyh^{-1}$)	E_{out} ($mSvy^{-1}$)	E_{in} ($mSvy^{-1}$)	ACED ($mSvy^{-1}$)	ELCR× 10^{-3}
C1	22.88	11.66	0.0143	0.0572	0.4759	1.50
C2	12.01	5.74	0.0070	0.0282	0.3564	1.12
C3	12.52	6.45	0.0079	0.0316	0.2831	0.89
C4	21.79	10.93	0.0134	0.0536	0.4946	1.56
C5	18.27	9.51	0.0117	0.0467	0.3793	1.19
C6	91.69	45.93	0.0563	0.2253	2.2254	7.01
C7	78.48	39.59	0.0486	0.1942	1.8511	5.83
C8	63.23	31.52	0.0387	0.1546	1.5403	4.85
C9	17.76	8.71	0.0107	0.0427	0.5858	1.85
C10	40.88	20.33	0.0249	0.0997	1.1779	3.71
C11	61.69	31.75	0.0389	0.1557	1.3034	4.11
Ave	40.11	20.19	0.0248	0.0990	0.9703	3.06
Min	12.01	5.74	0.0070	0.0282	0.2831	0.89
Max	91.69	45.93	0.0563	0.2253	2.2254	7.01

Table A.6: Average radiological hazard indices calculated from ^{232}Th, ^{40}K, and ^{226}Ra mean concentrations in khat from different countries.

Country	**Ra_{eq}**	**D**	**ACED**	**ELCR**	**Reference**
Kenya	150.55	72.02	36.51	27.79	(Njagi et al., 2022)
Ethiopia	34.41	16.77	7.71	26.98	(Techan, 2021)
Yemen	183.64	86.14	59.19	207.16	(Al-jalali & Shaltout, 2014)
Uganda	40.13	20.19	9.70	33.96	This study

Table A.7: The Radiological Toolbox-generated annual organ doses received from ingestion of ^{232}Th, ^{40}K, and ^{226}Ra in khat from the Dadamu-Sub-county.

Organ	Annual organ dose in (Sv)		
	^{40}K	**^{226}Ra**	**^{232}Th**
Adrenals	1.6469E-06	2.9684E-07	2.0164E-07
Urinary Bladder	2.0344E-06	2.8961E-07	2.0164E-07
Bone Surface	1.6146E-06	0.00008688	0.00006722
Brain	1.5823E-06	2.9684E-07	2.0164E-07
Breast	1.5823E-06	2.8964E-07	2.0164E-07
Esophagus	1.6146E-06	2.8965E-07	2.0164E-07
Stomach	1.8084E-06	2.9684E-07	2.0164E-07
Small Intestine	1.6469E-06	3.0408E-07	2.1282E-07
Upper Large Intestine	3.1323E-06	4.6336E-07	0.00000028
Lower Large Intestine	6.1355E-06	0.00000109	4.4243E-07
Colon	4.5209E-06	7.1676E-07	3.5284E-07
Kidneys	1.6146E-06	4.2716E-07	0.00000101
Liver	1.6146E-06	1.3032E-06	0.00000106
Muscle	1.6146E-06	2.8965E-07	2.0164E-07
Ovaries	1.6469E-06	2.9684E-07	0.00000062
Pancreas	1.6469E-06	2.8966E-07	2.016E-07
Red Marrow	1.6146E-06	6.2988E-06	0.00000263

Extratracheal Airways	1.6146E-06	2.8968E-07	2.0164E-07
Lungs	1.6146E-06	2.8963E-07	2.0164E-07
Skin	1.5500E-06	2.8964E-07	2.0164E-07
Spleen	1.6146E-06	3.8372E-07	2.016E-07
Testes	1.6146E-06	2.8969E-07	0.00000062
Thymus	1.6146E-06	2.8960E-07	2.0164E-07
Thyroid	1.6146E-06	2.8966E-07	2.0164E-07
Uterus	1.6469E-06	2.8962E-07	2.0164E-07
Remainder	1.6146E-06	2.896 8E-07	2.0723E-07

Table A.8: The factor loadings for the Principal components in (a) Soil and (b) khat.

(a) Loading factors for soil.

Variables	**PC 1**	**PC 2**
^{226}Ra	0.3635	0.5941
^{232}Th	0.3639	−0.6570
^{40}K	0.3725	0.4267
Ra_{eq}	0.3858	−0.1302
D_R	0.3686	−0.0737
E_{out}	0.3864	−0.0742
ELCR	0.3864	−0.0736
Percentage of variance explained	95.55%	3.71%

(b) Loading factors for khat.

Variables	**PC 1**	**PC 2**
^{226}Ra	0.2979	0.8525
^{232}Th	0.3275	−0.1319
^{40}K	0.3309	−0.3738
Ra_{eq}	0.3406	−0.1165
D_R	0.3401	−0.1425
E_{out}	0.4301	−0.1428
E_{in}	0.3401	−0.1426
ACED	0.3403	0.1441
ELCR	0.3403	0.1441
Percentage of variance explained	95.30%	3.63%